Advantages of second order work as a rational safety factor and stability analysis of a reinforced rock slope

Jie Hu, Zhaohua Li, Félix Darve, Jili Feng

▶ **To cite this version:**

Jie Hu, Zhaohua Li, Félix Darve, Jili Feng. Advantages of second order work as a rational safety factor and stability analysis of a reinforced rock slope. Canadian Geotechnical Journal, 2020, 57 (5), pp.661-672. ⟨10.1139/cgj-2019-0092⟩. ⟨hal-04919824⟩

HAL Id: hal-04919824

https://hal.science/hal-04919824v1

Submitted on 12 May 2026

HAL is a multi-disciplinary open access archive for the deposit and dissemination of scientific research documents, whether they are published or not. The documents may come from teaching and research institutions in France or abroad, or from public or private research centers.

L'archive ouverte pluridisciplinaire **HAL**, est destinée au dépôt et à la diffusion de documents scientifiques de niveau recherche, publiés ou non, émanant des établissements d'enseignement et de recherche français ou étrangers, des laboratoires publics ou privés.

Distributed under a Creative Commons CC BY 4.0 - Attribution - International License

Advantages of the second order work as a rational safety factor and stability analysis of a reinforced rock slope

Jie Hu[a], Zhaohua Li[a*], Félix Darve[b], Jili Feng[a]

a. State Key Laboratory for Geomechanics and Deep Underground Engineering, China University of Mining and Technology, Beijing, 100083, China

b. Grenoble CNRS, UMR 5521, 3SR, Grenoble Alpes University, Grenoble, France

Abstract: Landslides can be considered as a static-dynamic transition with the sudden release of kinetic energy. The sharp vanishing of the second-order work is also linked to it. In this study, the relation between the second-order work and the kinetic energy is reviewed, and 5 advantages of the normalized global second-order work (D^2Wn) as a factor of safety (FOS) are proposed and discussed, comparing with the FOS based on the strength reduction method. The D^2Wn is considered in the explicit algorithm of the FDM method, and its mesh-independence is numerically checked by a series of triaxial compression tests. By simulating the excavations of a reinforced rock slope, the stability analyses are performed using the D^2Wn and the traditional FOS, respectively. The D^2Wn is proven completely independent on the convergence criterion and more sensitive to the global failure. Finally, a recently-developed energy-absorbing cable is considered to support the studied rock slope. Its supporting effect is compared with that of the traditional cables.

Keywords: Second-order work; Factor of safety; Stability; Kinetic energy; CRLD cable; Numerical simulation

1. Introduction

Landslide is still a worldwide open problem. This problem can be divided into 2 major questions: stability analysis and reinforcement of slopes. Thus far, several methods have been developed to assess the stability of slopes, for example, the Strength Reduction (SR) (Griffiths and Lane 1999) and Limit Analysis (LA) methods (Davis and Selvadurai 2002). Failure mechanisms are determined with these methods, generally by using associated flow rules, when the corresponding stress states reach their yield surfaces (Note that the limit analysis is restricted to the normality rule, but standard strength reduction finite element analysis can be performed using a non-associated flow rule

(Tschuchnigg et al. 2015)). According to the results of the limit analysis, proposed by Adhikary and Dyskin (Adhikary and Dyskin 2007), the failure level was overestimated by at least 70%, compared with the experimental results. The results obtained in the stress-strain analysis were also doubtful, with a maximum error of 15%. Recently, the normalized quantity of the global second-order work D^2Wn was proposed for use as a Factor of Safety (FOS) for geotechnical structures, within the framework of the stress-strain analysis, because it can describe all the material instabilities by divergence, excluding the flutter instability (Prunier et al. 2016). Indeed, landslide mechanism is complicated, but the release of kinetic energy is always a significant and necessary feature for catastrophic fast landslides (Li et al. 2018). The instability process can be considered as a static-dynamic transition of the involved geomaterials, and the burst of kinetic energy corresponds to global failure (Nguyen et al. 2016). In this paper, the feasibility of the normalized global second-order work D^2Wn as a FOS is carefully discussed from an energy viewpoint. Furthermore, a detailed comparison between the D^2Wn and the traditional FOS is performed, and several advantages of the D^2Wn are summarized.

In addition to the stability analysis, the reinforcement of slopes is another major issue. The use of anchor cables is an effective and economic support technique for preventing the occurrence of landslides. The cables currently in use are generally classified into three types: strength, ductile, and energy-absorbing cables. Energy-absorbing cables have high strength and sufficient ductility (Chunlin Li 2010). In recent decades, many energy-absorbing bolts have been developed such as the Cone bolt (St-Pierre et al. 2009), Modified Cone Bolt (MCB) (Simser et al. 2007), Garford Solid Dynamic Bolt (GSDB) (Charette and Plouffe 2008), and D bolt (Chunlin Li 2010). Investigations on the new energy-absorbing support devices have made a significant contribution to safety in geotechnical engineering. However, the relationship between their tension (working resistance) and displacement still represents the traditional mode of elastic deformation-strain strengthening-strain softening. In this study, a recently-developed energy-absorbing cable, called the Constant-Resistance-Large-Deformation (CRLD) cable (He et al. 2014; Li et al. 2019a), is considered. Fig. 1 presents the structure of this cable. The CRLD cable is constituted principally by a thick-walled pipe, a piston-like cone body, and a cluster of steel strands. The strands are forged with the cone at one end and fixed by a nut at another end. The pipe is anchored in the country rock by using grouting material; thus, the CRLD cable is a two-point anchored cable. In case pull loading is exerted, a cone-pipe relative sliding will happen. The small-end diameter of the cone is designed to be slightly smaller than the inner diameter of the pipe, to facilitate the installation of the cone on the pipe. The large-end diameter is greater than the inner diameter of the pipe so that friction can be generated on the cone-pipe interface. In actual scenarios, with the above-mentioned structure, the CRLD cable can support large deformation with a maximum value of 2 m and provide constant resistance.

An index linked to the kinetic energy can be a proper FOS to evaluate stability, and CRLD cables can provide stronger reinforcement. In this paper, it is the first time one compares the D^2Wn with the traditional FOS in detail. The advantages of the D^2Wn, especially the independence on the convergence criterion, and its sensitivity to detect the approach of a global failure, are originally proposed and checked. In addition, the CRLD cable element is developed and verified, in the framework of the FLAC3D software, and the supporting effect of the CRLD cables is compared with that of the traditional ones, thanks to the second-order work.

This paper is organised as follows. In Section 2, the second-order work and its relation to kinetic energy are first briefly presented; second, the second-order work is implemented into the FLAC3D software, within the framework of an explicit algorithm; third, several triaxial compression tests of the sandstone are simulated to verify the implantation and the mesh-independence of the D^2Wn. Section 3 is devoted to prove the reliability and present the advantages of using the D^2Wn as a FOS. A stability analysis of a rock slope reinforced by traditional cables is performed, using the D^2Wn and the FOS based on the SR method, respectively. A series of excavations are carried out, and the evolutions of the two FOS are compared. In Section 4, the development of the CRLD cable element is presented, based on the original cable element of the FLAC3D software. Using the D^2Wn as the safety factor, the stabilities of the rock slope reinforced by traditional and CRLD cables, respectively, are compared and discussed. Section 5 presents the conclusions of this study.

2. Computation of second-order work based on explicit dynamic algorithm

In this work, the background of the second-order work is reviewed. The calculation of the second-order work is discussed within the framework of an explicit algorithm, and its implementation into the FLAC3D software is validated.

2.1 Brief review of the second-order work criterion and its relation to kinetic energy

Instability problems can be principally classified into two categories: geometric instabilities related to specific boundary conditions and material instabilities related to particular material properties or states. The latter consists of two types: divergence instabilities, where strains increase suddenly and monotonously to high values, and flutter instabilities, corresponding to cyclical strains with increasing amplitude (Bigoni and Noselli 2011). Geomaterials exhibit a non-associated behaviour and can undergo localised or diffuse failure, before the classical plastic limit criterion is satisfied. Previous studies have proven the second-order work criterion to be reliable for describing all divergence instabilities, excluding flutter instabilities, and can be considered as the instability criterion best describing the physical phenomena (Li et al. 2016; Nicot and Darve 2011; Darve et al. 2004; Nicot and Darve 2007; Darve et al. 2007; Sibille et al. 2008; Prunier et al. 2009). It is expressed using Eq. (1a), in the framework of small strain assumption and by neglecting geometric effects. Its normalized form to improve the readability of numerical results can be written by Eq. (1b).

$$d^2w = d\boldsymbol{\sigma}'_{ij} d\boldsymbol{\varepsilon}_{ij} \qquad (1a)$$

$$d^2w_{norm} = \frac{d^2w}{\|d\boldsymbol{\sigma}'_{ij}\| \|d\boldsymbol{\varepsilon}_{ij}\|} \qquad (1b)$$

where d^2w is the second-order work, and d^2w_{norm} is its normalized form, whose value is limited from -1 to 1. $\|d\boldsymbol{\sigma}'_{ij}\|$ and $\|d\boldsymbol{\varepsilon}_{ij}\|$ denote the norms of effective stress increment and strain increment, respectively. The geomaterial is strictly unstable when $d^2w_{norm} \leq 0$ in the current loading direction (Nicot and Darve 2011; Darve et al. 2004; Nicot and Darve 2007; Darve et al. 2007;

Sibille et al. 2008; Prunier et al. 2009).

To solve the boundary value issues, the general form of normalized global second-order work, expressed in Eq. 2a, can be rewritten after space discretization, as follows (Eq. 2b):

$$D^2W_n = \frac{\int_V d^2w dV}{\int_V \|d\boldsymbol{\sigma}\| \cdot \|d\boldsymbol{\varepsilon}\| dV} \qquad (2a)$$

$$D^2W_n = \frac{\sum_i^n (d^2W_i \cdot V_i)}{\sum_i^n \int_{V_i} \|d\boldsymbol{\sigma}_i'\| \|d\boldsymbol{\varepsilon}_i\| dV_i} \qquad (2b)$$

where D^2W_n is the normalized global second-order work and V_i the volume discretised in the numerical model. This quantity can be used to analyse the global stability of the geomaterial, and Prunier used it as a FOS in a finite element code (Prunier et al. 2016).

In this study, the second-order work is calculated using the FLAC3D software, in the framework of the explicit algorithm. The equation of motion (see Eq. (3)) is used to solve static problems, and a damping term has to be considered to ensure convergence at each loading step (Itasca Consulting Group, Inc 2012).

$$div\boldsymbol{\sigma}' + b = \rho\ddot{u} + \boldsymbol{F_D} \qquad (3)$$

where ρ is the density, and $\boldsymbol{\sigma}'$and b are the effective stress matrix and force vectors, respectively. $\ddot{u}$ is the acceleration vector, and $\boldsymbol{F_D}$ the damping force vector. It was assumed that density ρ is a constant and the time derivative of Eq. (3) is given, by multiplying the velocity vector $\dot{\boldsymbol{u}}$ on the left and right sides, as a scalar product:

$$(div\dot{\boldsymbol{\sigma}}' + \dot{b})\dot{u} = \rho\ddot{\boldsymbol{u}}\dot{u} + \dot{\boldsymbol{F}}_{\boldsymbol{D}}\dot{u} \qquad (4)$$

By introducing the second derivative of kinetic energy $\ddot{E}_c = \rho\|\ddot{\boldsymbol{u}}^2\| + \rho\ddot{\boldsymbol{u}}\dot{u}$ and the Gauss divergence theorem, the direct relation between the second-order work and kinetic energy can thus be obtained, as follows:

$$\frac{d^2W}{dt^2} = div(\dot{\boldsymbol{\sigma}}'\dot{u}) + \dot{b}\dot{u} - \ddot{E}_c + \rho\|\ddot{\boldsymbol{u}}^2\| - \dot{\boldsymbol{F}}_{\boldsymbol{D}}\dot{u} \qquad (5)$$

where dt is the time step, interpreted in the numerical computations as Δt. Considering Taylor's expansion and considering only the first and second derivatives, Eq. (5) can be rewritten as follows:

$$E_c(t + \Delta t) - E_c(t) \approx \dot{E}_c(t)\Delta t + \frac{1}{2}(\Delta t)^2\left(div(\dot{\boldsymbol{\sigma}}'\dot{u}) + \dot{b}\dot{u} + \rho\|\ddot{\boldsymbol{u}}^2\| - \dot{\boldsymbol{F}}_{\boldsymbol{D}}\dot{u}\right) - \frac{1}{2}d^2W \qquad (6)$$

$\frac{1}{2}(\Delta t)^2 div(\dot{\boldsymbol{\sigma}}'\dot{u})$ can be considered as a boundary term, involving the control parameters (the displacement $\boldsymbol{u}$ and the effective stress $\boldsymbol{\sigma}'$, corresponding to the external force), and $\frac{1}{2}(\Delta t)^2\rho\|\ddot{\boldsymbol{u}}^2\|$ and $\frac{1}{2}(\Delta t)^2\dot{\boldsymbol{F}}_{\boldsymbol{D}}\dot{u}$ are the inertial and damping terms, respectively. In accordance with the explicit dynamic algorithm, once a load is exerted, a solution with a positive inertial term is obtained. In other words, the equilibrium state has to be ensured after a few calculation steps, to progressively remove the inertial term by using the damping term. During these calculation steps, the load on the boundary is constant. Considering a constant body force, Eq. (6) can be simplified as follows:

$$\Delta E_c(\Delta t) = E_c(t + \Delta t) - E_c(t) \approx -\frac{1}{2}d^2W + \dot{E}_c(t)\Delta t + \frac{(\Delta t)^2}{2}\left(\rho\|\ddot{\boldsymbol{u}}^2\| - \dot{\boldsymbol{F}}_{\boldsymbol{D}}\dot{u}\right) \qquad (7)$$

Hence, under a dead external load and for quasi-static loading conditions, the increment of kinetic energy will depend only on the second-order work and the damping term. As long as the internal second-order work is positive, the kinetic energy will not take any positive value before reaching the equilibrium state with all terms vanishing. However, as soon as the internal second-order work is taking negative values in relation with the current material properties and the loading path, then the kinetic energy will have a strictly positive value, any static equilibrium state can no more be reached and a dynamic failure will occur. Eq. (7) is significant for studies on the kinetic energy release from geomaterials, and is potential to describe underground excavation or rock burst processes.

2.2 Validation of second-order work in homogenous material

To ensure the numerical cost, the local second-order work is calculated, based on the existing code of the Mohr-Coulomb model (written using C++ language). The corresponding dynamic link library (DLL) is developed, and the local second-order work in each zone can be invoked at each calculation step. Using the code by FISH language (see the appendix A1), the global second-order work is then determined, and the second-order work is thus implanted into the FLAC3D software within the framework of an explicit dynamic algorithm. In this sub-section, the verification of the implantation and the mesh-independence of the second-order work are performed via several triaxial compression tests of the homogenous sandstone sample.

2.2.1 Validation of implantation

As shown in Fig. 2a, the homogenous sandstone sample, with dimensions of 5 cm × 5 cm × 10 cm, is first initialised under three different confined pressures (0, 10, and 20 MPa), and a constant velocity of 10^{-4} mm/s is then applied in the z-direction. The tests are controlled by the sufficiently small strain increment (the corresponding strain rate is 10^{-6} /s), and the dynamic effect is thus negligible. To discuss the rationality of the D^2Wn as a FOS from an energy viewpoint (that from a viewpoint of bifurcation failure has been performed by Prunier (Prunier et al. 2016)), and to simplify the mechanical parameters involved in the numerical calculations, a relatively simple constitutive model is used. The perfect elastic-plastic model with the Mohr-Coulomb criterion is used to describe the mechanical behaviour of the sample, and the mechanical parameters are summarised in Table 1. It should be noted that the dilatancy angle is equal to the friction angle, according to Table 1. Thus, the studied material is associated, and the constitutive stiffness matrix satisfies the major symmetry conditions. Hence, failure will occur only if the Mohr-Coulomb criterion is satisfied, and the second-order work criterion is equivalent to the Mohr-Coulomb criterion (Nicot and Darve 2011; Prunier et al. 2009). Indeed, due to the lack of hardening and the use of a perfect elastic-plastic model, the failure will also occur only on the plasticity criterion, in case of a non-associative constitutive model.

Regarding the above-mentioned sandstone sample, the strength can be estimated according to the Mohr-Coulomb circle. The plateau values of σ_z are 82, 138, and 157 MPa, corresponding to the confined pressures of 0, 10, and 20 MPa, respectively. As shown in Fig. 3, σ_z initially increase and then remains constant at a velocity of 10^{-4} mm/s, once its corresponding plateau is reached. It means that the plastic limit, indicated by the Mohr-Coulomb criterion, is satisfied. In the meantime, the

normalized global second-order work D^2Wn, calculated using Eq. (2), also vanishes. In other words, the vanishing of D^2Wn coincides well with the plastic limit, because of the symmetry of stiffness matrix of the associated material. In addition, D^2Wn is equal to the cosine of the angle between the stress and strain increment vectors, for homogeneous conditions. Hence, a positive value of D^2Wn is observed in elastic regime (see Fig. 3), because the vectors of stress and strain increments are quasi parallel. It is a bit lower than 1 (about 0.94), due to the Poisson's ratio effect. Then it decreases sharply and remains close to 0, once the failure occurs, because the vector of the stress increment is vertical in Rendulic plane, and that of the strain increment is perpendicular to Mohr-Coulomb line.

2.2.2 Mesh independence

As shown in Fig. 2b, the mesh is refined with 125 and 1000 elements, respectively, based on the model shown in Fig. 2a. Sample compression tests are performed, and the mesh independence of the index is validated. Fig. 4 shows the numerical results of the D^2Wn, and a good agreement with 3 D^2Wn is observed, which means that D^2Wn does not depend on the mesh, especially before the global failure occurs.

3. Stability analyses of a reinforced rock slope using D^2Wn as a new FOS

In this section, the reliability and advantages of the normalized global second-order work D^2Wn as a FOS is presented in an inhomogeneous boundary value problem. The new FOS has some significant advantages compared with the traditional ones, as follows.

- In terms of computational accuracy, the value of the traditional FOS, for example, the one based on the SR method, is dependent on the mesh design (Cheng et al. 2007; Wei et al. 2009), but D^2Wn is mesh-independent. It can effectively avoid the numerical error caused by grid division and it gives more objective results, which has been shown in Section 2.2.
- The calculation of D^2Wn is based on the constitutive stress-strain relation; it is the most conservative criterion for bifurcation failure. It can describe all the material bifurcations by divergence, as Lerbet (Lerbet et al. 2015) has shown by variational methods and Prunier has presented (Prunier et al. 2016), while the traditional FOS is only available for the failures at plastic limit.
- The traditional FOS is sensitive to the convergence criterion, which is an artificial parameter, but D^2Wn is a more objective index, and is independent on that factor. It is only influenced by the damping coefficient (because it is linked to the kinetic energy), which is a physical parameter.
- The D^2Wn can be calculated, in consideration of the large deformation and dynamics, but the FOS based on the SR method is limited in the static analysis with a small deformation assumption (Wei et al. 2009).
- The D^2Wn is more sensitive when the geotechnical structure is approaching the global failure, while in the case of traditional FOS, the variation is more confused.

The first 2 advantages have been proven, and the last 3 will be verified in next paragraphs. Thus, the normalized global second-order work is more general and physical as a FOS.

3.1 Model description

This paper considered a rock slope on the north bank of the opencast gold mine in Inner Mongolia of China as a benchmark, which lost the stability in April 2017, due to the excavation of about 35 m on the toe of the slope. Fig. 5 shows the studied area of the rock slope. In I_1W and I_2 areas, 39 and 102 anchor cables are installed, respectively, and 60 bolts are distributed in I_1E area. The geometrical and mechanical parameters of the supports are listed in Table 2.

In line with the actual slope shape, several platforms are considered along the slope surface of the numerical model, with a slope angle of approximately 43°, slope height of 84 m and top length of 50 m. To improve the calculation accuracy and avoid boundary effect, the length and thickness of the model were set as 179 m and 95 m, respectively. The three-direction displacement constraint at the bottom of the numerical model, and the normal lateral displacement constraint at the side of the model are assigned, whereas the remainder is free. The FDM model of the rock slope is thus established as shown in Fig. 6, and a perfect elastic-plastic model with Mohr-Coulomb criterion is used. The corresponding physical and mechanical parameters of the slope rock mass are determined in line with the previous geotechnical report, and are listed in Table 3. For the sake of simplicity and considering the calculation cost, the actual mining operation is simplified to a 12-step stratified excavation with a height of 3 m. Fig. 6 shows the layout of the numerical model, and the position of each cable (bolt) is identical to that of in-situ, as shown in Fig. 5.

3.2 Stability analysis of the reinforced rock slope using D^2Wn and the FOS proposed by FLAC3D software

In the small strain mode, 12 excavations at toe of the rock slope are progressively performed. Before the excavation process, gravity is first initialized. After each excavation, some calculation steps are needed to damp the kinetic energy, under a dead external load. For a given damping coefficient, if the kinetic energy finally decreases to a sufficiently small value due to the damping effect, the slope is considered stable, otherwise, it is unstable. As shown in Figs. 7a-b, the evolutions of the released kinetic energy after each excavation are presented. As the excavation proceeded, the rock slope remained in equilibrium states under the first seven excavations: the value of the kinetic energy increased slightly after each excavation, and then decreased close to 0 due to the damping effect (see Fig. 7a). For the last five excavations, the kinetic energy rose after each excavation, and then approached under the dead loading to constant values with slight oscillations (within 150000 steps after each excavation), which were larger and larger with excavation depth (see Fig. 7b). According to Eq. (7), the phenomena under the dead load can be explained by the damping effect. A positive second-order work induces a decreasing increment of kinetic energy, in absence of the inertial and damping terms. However, in the explicit algorithm of the FLAC3D software, these 2 terms are present. Consequently, if $\frac{(\Delta t)^2}{2}\left(\rho\|\ddot{\boldsymbol{u}}^2\| - \dot{\boldsymbol{F}}_{\boldsymbol{D}}\dot{u}\right) > \frac{1}{2}d^2W$, $\dot{E}_c(t+\Delta t)\Delta t$ is positive, and the

geomaterial tends to be unstable; otherwise, it may tend to be stable. A shallower excavation corresponds to a smaller $\rho\|\ddot{\boldsymbol{u}}^2\| - \dot{\boldsymbol{F}}_{\boldsymbol{D}}\dot{\mathrm{u}}$ term, so the kinetic energy may possibly decrease. A deeper excavation corresponds to a larger inertial term $\rho\|\ddot{\boldsymbol{u}}^2\|$ and a greater oscillation of the term $\rho\|\ddot{\boldsymbol{u}}^2\| - \dot{\boldsymbol{F}}_{\boldsymbol{D}}\dot{\mathrm{u}}$, so the kinetic energy increases with oscillations. When the kinetic energy is sufficiently large, the system does not satisfy the convergence rule of the FLAC3D software (the kinetic energy will never be damped to vanish).

Figs. 7c-d show the evolutions of the D^2Wn after each excavation. A comparison of the result with the one in Fig. 7a indicates an opposite trend between the kinetic energy and the normalized global second-order work D^2Wn. D^2Wn decreases while the kinetic energy increases gradually with slope excavation. For the last five excavations, the calculation cannot converge, under the convergence criterion with an assigned value of 1×10^{-5}. It means that the rock slope loses stability since the 8th excavation step. This is the conventional instability criterion during the numerical analysis. The kinetic energy, released at the 8th excavation step, is not too large considering the seize of the slope (approximately $1 \times 10^6 m^3$), but it can be considered that the instability occurs according to the traditional method of the FLAC3D software, taking into account the actual convergence criterion; however, the values of D^2Wn stay constant with a positive value, until the 12th excavation step, which means the rock slope remains stable, until the last excavation. It should be noted that the second-order work is influenced by the damping coefficient, which is a physical parameter. The D^2Wn is thus more rational as a FOS. In addition, when the kinetic energy of the system is at its most important value, the system is in its most unstable state. It can be seen from Fig. 7b that the corresponding D^2Wn remains constant at this time; thus, the lowest value of D^2Wn can be taken as the new FOS in this study.

The maximum unbalanced forces after each excavation are presented in Figs. 8. For the first 7 excavations, the maximum unbalanced forces vanish quickly; for the last 5 ones, they increase and keep a constant value with very large oscillations. The phenomena are consistent with the kinetic energy (see Figs. 7 a and b).

Figs. 9I present the evolution of the normalized local second-order work (calculated by Eq. 1b), which describes the development of the unstable zones, with the excavations. According to Figs. 9I, the unstable zone firstly appears in the fault, along the fault-strongly crushed schist interface, where the mechanical parameters are weak. With the depth of excavation, the unstable zones progressively develop and enlarge, on the toe of the slope and along the shear band in the fault (see Fig. 9Ib). After the 12th excavation step (see Fig. 9Ic), a thorough unstable zone is developed, corresponding to the global instability of the rock slope. Figs. 9II give the development of the maximum shear strain, and a good agreement with the unstable zone, indicated by d^2w_{norm}, is observed.

3.3 Comparison of the evolutions of the two FOSs

The above-mentioned rock slope stability is re-analyzed using a traditional FOS, proposed by the FLAC3D software. This FOS is based on the strength reduction method, in which the shear strength

of the studied material is progressively reduced to approach a state of limit equilibrium. A series of calculations should be carried out. The trial values are used to reduce the strength parameters, until critical state is found and failure occurs. The ratio of the actual strength parameter to the critical one is considered as the FOS.

Figs. 10 give the comparisons between D^2Wn and the FOS proposed by the FLAC3D software, under different convergence criteria, and it should be noted that there is a difference between the D^2Wn with the classical FOS: the former varies between -1 and 1, and a positive value stands for a global stable state, while a vanishing value means the global instability; however, the latter is always positive, and 1 is the limit to distinguish the stable from the unstable state. According to Figs. 10, first, both the two factors exhibit the same trend, and they decrease as the excavations are progressively carried out; second, D^2Wn decreases slightly before the 8th excavation step, and is more sensitive, when the global instability of the rock slope is approached (after the 8th excavation step). The reason is that an approaching instability corresponds to an increasing released kinetic energy, and D^2Wn can obviously indicate it. Regarding the FOS of FLAC3D software, a contrary phenomenon is observed. It decreases sharply before the 8th excavation, and then evolves slightly; third, the evolution of D^2Wn does not change, under the different convergence criteria (1×10^{-5} and 3×10^{-4}). However, the traditional FOS is evidently influenced, according to Figs. 10a and b.

As a conclusion, compared with the traditional FOS, D^2Wn is tightly linked to the kinetic energy, and is independent on the mesh and the convergence criterion. Hence, it is more physical and reliable as a FOS.

4. Reinforcement effect using traditional and CRLD supports

In this section, the development of the CRLD cable element, based on the existing cable element of the FLAC3D software is first presented. And then the stability analyses of the rock slope, reinforced by the traditional and CRLD cables, respectively, are performed, by using the new FOS.

4.1 CRLD cable element and its validation

To describe the mechanical behaviour of large deformation and constant resistance, a tension-deformation relation of the CRLD cable is proposed in Eq. (8). In case that the load F on the CRLD cable is smaller than the constant resistance F_{CR}, the tension-deformation relation is identical to the existing elastic one of the FLAC3D software ($F=KU$), with K the cable rigidity and U the axial deformation of the cable. In case that F is larger than F_{CR}, and U is smaller than the tolerance of the axial deformation U_M, the tensile strength of the cable F_S is assigned to be F_{CR}, to ensure that the tensile force remains equal to the value of F_{CR}. In case that F is smaller than F_S and U becomes larger than U_M, F_S is re-assigned to be the initial tensile strength, and the tensile load F can thus continue to increase with the deformation U. Finally, in case of F exceeds the tensile strength, F_S is assigned to vanish, which means the failure of the cable.

$$F = \begin{cases} KU & (F \le F_{CR}) \\ F_{CR} & (F > F_{CR}, U \le U_M) \\ KU & (F_{CR} < F \le F_S, U > U_M) \\ 0 & (F > F_S) \end{cases} \quad (8)$$

To verify the tension-deformation relation of the CRLD cable and compare with the one of the traditional cable, in the framework of the FLAC3D software, the numerical pull-out tests are performed, as shown in Fig. 11. The cross-sectional area of both the cables is 0.2238 m^2, the Young's modulus is 205 GPa, the length of the cable is 27 m, the tensile strength is 1500 kN, and the constant resistance and the maximum deformation of the CRLD are 850 kN and 1000 mm, respectively. The two ends of the cable element are fixed in the rigid hexahedron zone. One zone is fixed, and the other is stretched with a constant velocity of 20 mm/min, until the failure occurs.

In Fig. 12, the numerical results of the tension-deformation relations for the traditional cable (blue dotted line) and CRLD one (red continuous line) are presented, and compared with the corresponding experimental result for the CRLD cable (black continuous line). On one hand, the CRLD cable exhibits a good ductility. The tensile force linearly increases, exhibiting an elastic behaviour, and a constant resistance of 850 kN is then ensured during the large deformation stage, in which the energy-absorbing can be realized. Once the maximum deformation of 1000 mm is reached, the numerical tensile force continues to increase, because the blockage of the cone by the pallet (see Fig. 1) is taken into account in the numerical cable model. Finally, a sudden decrease appears, when the tensile strength of 1500 kN is reached (the pallet is not taken into account in the laboratory tests, and the cone is directly pulled out of the pipe, so the tensile load decreases after the constant resistance (Li et al. 2019b)). On the other hand, the traditional cable presents a fragile behaviour.

4.2 Stability analysis of the rock slope reinforced by the different cables using the new FOS

Based on the numerical model in Fig. 7, and replacing all the traditional cables by the CRLD ones, a rock slope reinforced by the CRLD cables is simulated. Using the parameters in Table 2, the stability analyses of the rock slope, reinforced by the traditional and CRLD cables, respectively, are performed in the large strain mode. As shown in Fig. 13, the evolutions of D^2Wn, with the two different support systems, are obtained and compared.

As can be seen from Fig. 13, with the increase in the excavation depth of the rock slope, the normalized global second-order work of the rock slope D^2Wn exhibits a downward trend, in both the anchorage systems. It indicates that the stability of the rock slope is degraded by the progressive excavations. With the same excavation depth, the value of D^2Wn of the CRLD anchorage system is always larger than that of the traditional cable anchorage system. After the completion of the 6th excavation step, both the two D^2Wn begin to sharply decrease, and the kinetic energy of the slope starts to rapidly increase. For the traditional supporting system, the D^2Wn declines more quickly. Especially, after the 11th excavation step, the D^2Wn decreases to a negative value within the

traditional supporting system, which means that the rock slope reinforced by the traditional supporting system is globally unstable. However, the CRLD supporting system can still maintain the stability of the slope, which corresponds to a positive D^2Wn of about 0.4. These results show that the CRLD cables considerably improve slope stability.

Figs. 14I and II present the displacement contours of the slope, reinforced by the traditional and CRLD cables, respectively. As shown in Figs 14Ia and 14IIa, the displacement fields are almost identical, after the 1st excavation step. Because the perturbation of the excavation is small, both the cables and the country rock are in elastic regime. After the 7th excavation step, a significant displacement is observed nearby the surface of the slope, reinforced by the traditional cables (see Fig. 14Ib), and the D^2Wn starts to sharply decrease, as shown in Fig. 12. However, the maximum displacement of the slope under the CRLD cable reinforcement is only 3.414×10^{-1} m (see Fig. 14IIb), and only a slight decrease of the D^2Wn is presented according to Fig. 12. After the 12th excavation step, the slope with the traditional reinforcement exhibits a global instability, while that with the CRLD reinforcement is globally stable (see Figs. 14c).

Fig. 15 presents the state of the two reinforcement systems after the 12th excavation. Regarding the CRLD reinforcement system, the cables in the 1st, 2nd, 3rd, and 6th rows still work (see Fig. 14a). However, all the traditional cables fail (see Fig. 14b), under identical conditions. The ductile behaviour of the CRLD cables is thus proven.

5. Conclusion

In this study, the second-order work is implanted in the 3D explicit dynamic algorithm, and its advantages as a new FOS are discussed and validated in detail. Then, a recent-developed energy-absorbing cable, the CRLD cable is numerically simulated in the FLAC3D software, and its reinforcement effect is proven, compared with the traditional one.

The relation between the second-order work and the kinetic energy is reviewed in detail, and the advantages of the normalized global second-order work as a FOS are summarised. Compared with the traditional FOS of the FLAC3D software, it is independent on the mesh design and convergence criterion. It is more general, due to its tight relation to the kinetic energy, whereas the value of the traditional one is dependent to the above-mentioned 2 factors; third, it is available during the calculation taking into account the large deformation, whereas the traditional one can only be used within the small deformation assumption; fourth, it is more sensitive when the geotechnical structure is approaching the global failure, which may be useful for the prediction of geo-hazards; fifth, it can describe all bifurcation failures by divergence, excluding the flutter failure. The first four advantages are then carefully validated in a sandstone sample (homogenous medium) and a reinforced rock slope model (inhomogeneous medium), while the fifth advantage has been verified by Prunier (Prunier et al. 2016), and proven mathematically by variational methods (Lerbet et al. 2015). It is worth noting that the FOS is a basic index in geotechnical engineering. The comparison and

discussion of the FOSs are significant for the geotechnical design.

Finally, the CRLD cable element is simulated, based on the existing cable element of the FLAC3D software, and its ductility with a constant resistance is then validated via the numerical pull-out tests. The stability analyses of the rock slope reinforced by traditional and CRLD cables, respectively, are carried out and compared each other. The CRLD cables exhibit a better performance, and the slope reinforced by them exhibits a better stability, according to the new FOS.

Nomenclature:

D^2Wn normalized global second-order work;
d^2w second-order work;
d^2w_{norm} normalized localsecond-order work;
ρ density
$\boldsymbol{\sigma'}$ effective stress matrix
b force vector
$\boldsymbol{U}$ displacement
ü acceleration vector
$\boldsymbol{F_D}$ damping force vector
$\ddot{E}_c$ second derivative of the kinetic energy
Δt time step
F load on the CRLD cable
F_{CR} constant resistance
K rigidity of cable
U axial deformation of cable
U_M tolerant value of axial deformation of cable
F_S tensile strength of cable.

Adhikary, D.P., and Dyskin, A.V. 2007. Modelling of Progressive and Instantaneous Failures of Foliated Rock Slopes. Rock Mechanics and Rock Engineering, **40**(4): 349-362.

Bigoni, D., and Noselli, G. 2011. Experimental evidence of flutter and divergence instabilities induced by dry friction. Journal of the Mechanics and Physics of Solids, **59**(10): 2208-2226.

Charette, F., and Plouffe, M. 2008. A new rock bolt concept for underground excavations under high stress conditions. *In* Sixth Int. Symp. on Ground Support in Mining and Civil Engineering Construction. SAIMM, Johannesburg. pp. 225-240.

Cheng, Y.M., Lansivaara, T., and Wei, W.B. 2007. Two-dimensional slope stability analysis by limit equilibrium and strength reduction methods. Computers and Geotechnics, **34**(3): 137-150.

Chunlin Li, C. 2010. A new energy-absorbing bolt for rock support in high stress rock masses. International Journal of Rock Mechanics and Mining Sciences, **47**(3): 396-404.

Darve, F., Servant, G., Laouafa, F., and Khoa, H.D.V. 2004. Failure in geomaterials: continuous and discrete analyses. Computer Methods in Applied Mechanics and Engineering, **193**(27): 3057-3085.

Darve, F., Sibille, L., Daouadji, A., and Nicot, F. 2007. Bifurcations in granular media: macro- and micro-mechanics approaches. Comptes Rendus Mécanique, **335**(9): 496-515.

Davis, R.O., and Selvadurai, P. 2002. Plasticity and Geomechanics. Cambridge University Press.

Griffiths, D., and Lane, P.A. 1999. Slope stability analysis by finite elements. Geotechnique, **49**(3): 653-654.

He, M., Gong, W., Wang, J., Qi, P., Tao, Z., Du, S., and Peng, Y. 2014. Development of a novel energy-absorbing bolt with extraordinarily large elongation and constant resistance. International Journal of Rock Mechanics and Mining Sciences, **67**: 29-42.

Itasca Consulting Group Inc 2012. FLAC3D—fast Lagrangian analysis of continua in three-dimensions, ver. 5.0., Minneapolis, USA.

Lerbet, J., Challamel, N., Nicot, F., and Darve, F. 2015. Variational formulation of divergence stability for constrained systems. Applied Mathematical Modelling, **39**(23): 7469-7482.

Li, Z., Dufour, F., and Darve, F. 2016. Hydro-elasto-plastic modelling with a solid/fluid transition. Computers and Geotechnics, **75**: 69-79.

Li, Z., Jiang, Y., Tao, Z., and He, M. 2019a. Monitoring prediction of a rockslide in an open-pit mine and numerical analysis using a material instability criterion. Bulletin of Engineering Geology the Environment, **78**(3): 2041-2053.

Li, Z., Lv, Q., Zhu, H., Hu, J., Feng, J., and He, M. 2019b. Laboratory testing and modeling of a high-displacement cable bolt. **19**(7): 04019078. doi:10.1061/(ASCE)GM.1943-5622.0001472.

Li, Z.H., Jiang, Y.J., Lv, Q., Sousa, L.R., and He, M.C. 2018. Consistent modeling of a catastrophic flowslide at the Shenzhen landfill using a hydro-elasto-plastic model with solid–fluid transition [journal article]. Acta Geotechnica, **13**(6): 1451-1466.

Nguyen, H.N.G., Prunier, F., Djeran-Maigre, I., and Nicot, F. 2016. Kinetic energy and collapse of granular materials. Granular Matter, **18**(1): 5.

Nicot, F., and Darve, F. 2007. A micro-mechanical investigation of bifurcation in granular materials. International Journal of Solids and Structures, **44**(20): 6630-6652.

Nicot, F., and Darve, F. 2011. Diffuse and localized failure modes: Two competing mechanisms. International Journal for Numerical and Analytical Methods in Geomechanics, **35**(5): 586-601.

Prunier, F., Laouafa, F., Lignon, S., and Darve, F. 2009. Bifurcation modeling in geomaterials: From the second-order work criterion to spectral analyses. International Journal for Numerical and

Analytical Methods in Geomechanics, **33**(9): 1169-1202.

Prunier, F., Chomette, B., Brun, M., and Darve, F. 2016. Designing geotechnical structures with a proper stability criterion as a safety factor. Computers and Geotechnics, **71**: 98-114.

Sibille, L., Donze, F., Nicot, F., Chareyre, B., and Darve, F. 2008. Bifurcation detection and catastrophic failure. Acta Geotecnica, **3**(1): 14-24.

Simser, B., Parrott, T., Turcotte, P., Mercier-Langevin, F., and Andrieux, P. 2007. Field Behaviour and Failure Modes of Modified Conebolts at the Craig, LaRonde and Brunswick Mines in Canada. *In* Challenges in deep and high stress mining, Australian Centre for Geomechanics. *Edited by* J.H. Y. Potvin, D. Stacey (Eds.), Perth. pp. 347-354.

St-Pierre, L., Hassani, F.P., Radziszewski, P.H., and Ouellet, J. 2009. Development of a dynamic model for a cone bolt. International Journal of Rock Mechanics and Mining Sciences, **46**(1): 107-114.

Tschuchnigg, F., Schweiger, H.F., and Sloan, S.W. 2015. Slope stability analysis by means of finite element limit analysis and finite element strength reduction techniques. Part I: Numerical studies considering non-associated plasticity. Computers and Geotechnics, **70**: 169-177.

Wei, W.B., Cheng, Y.M., and Li, L. 2009. Three-dimensional slope failure analysis by the strength reduction and limit equilibrium methods. Computers and Geotechnics, **36**(1): 70-80.

Fig.1: Structure scheme of the CRLD cable

Fig. 2: a) FDM model of triaxial compression tests for homogeneous sandstone sample, with confined pressures of 0, 10 and 20 MPa; b) FDM model of simple compression tests for homogeneous sandstone sample, with refined meshes with 125 and 1000 elements.

Fig. 3: Validation of the second-order work criterion for associated material under different confined pressures (0, 10 and 20 MPa). The 3 continuous and dashed curves stand for the evolutions of σ_z and D^2Wn under different confined pressures, respectively.

Fig. 4 Agreement of the D^2Wn with 3 different meshes

Fig. 5 Studied area of rock slope

Fig. 6 Boundary conditions and geometry of the initial rock slope and the layout of the cable (bolt). Model broadsides are fixed in the outer normal direction, and the bottom edge is fixed in three directions. E stands for the excavated layers, and the following numbers denotes the order of the excavations.

Fig.7 Evolutions of kinetic energy and D^2Wn after each excavation: (a) Kinetic energy during the first 7 excavations, and (b) the last 5 excavations; (c) D^2Wn during the first 7 excavations, and (d) the last 5 excavations

Fig. 8 Evolutions of maximum unbalanced force (a) during the first 7 excavations, and (b) the last 5 excavations

Fig. 9 Contour of (I) normalized local second-order work d^2w_{norm} and (II) maximum shear strain, after the (a) 1st (b) 7th and (c) 12th excavation step, respectively

Fig. 10 Evolutions of D^2Wn and FOS (SR method) with the convergence criterion of (a) 1e-5 and (b) 3e-4

Fig. 11 Pull-out test model of cables

Fig. 12 Tension load-deformation curves of the traditional and CRLD cables

Fig. 13 Evolutions of D^2Wn with the CRLD and traditional cables

Fig. 14 Displacement contours of the slope, reinforced by (I) the traditional cables and (II) the CRLD cables, respectively, after (a) the 1st, (b) 7th and (c) 12th excavation.

Fig. 15 Working condition of (a) the CRLD cable reinforcement system, and (b) the traditional cable reinforcement system, after the 12th excavation

Table 1 Mechanical parameters of the sandstone sample

Young's modulus	29.4 GPa
Poisson's ratio	0.25
Friction angle	40°
Dilation angle	40°
Density	1842 g/cm^3
Cohesion	20.0 MPa
Tension	10.3 MPa

Table 2 Physical and mechanical parameters of cables and bolts

	Tensile strength (kN)	Young's modulus (GPa)	Length (m)	Pre-stress (kN)	Cross section (m^2)	Constant resistance (kN)	Tolerant deformation (mm)
CRLD cable	1500	205	27	750	0.2238	850	1000
Traditional cable	1500	205	27	750	0.2238	-	-
Traditional bolt	800	205	8	0	0.373e-3	-	-

Table 3 Physical and mechanical parameters of involved rock mass

	Density (g/cm^3)	Young's modulus (GPa)	Poisson's ratio	Cohesion (Pa)	Friction angle (°)	Tensile strength (Pa)
Crushing schist	2.7	4.54	0.25	4.0e5	35	1.2e5
Strongly crushing schist	2.5	4.11	0.30	1.5e5	28	1.0e5
Fault	2.4	2.5	0.35	0.2e5	18	1.0e4
Excavation area	2.5	4.11	0.30	1.5e5	28	1.0e5

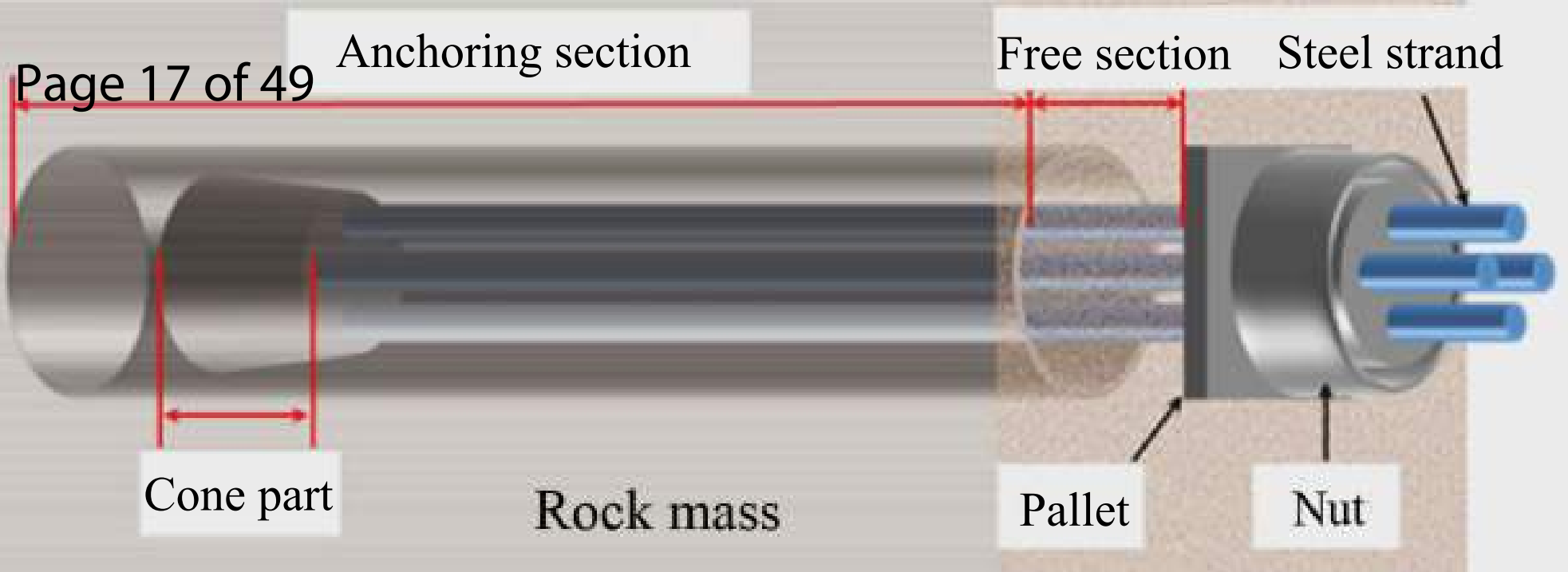
Anchoring section
Free section
Steel strand
Cone part
Rock mass
Pallet
Nut

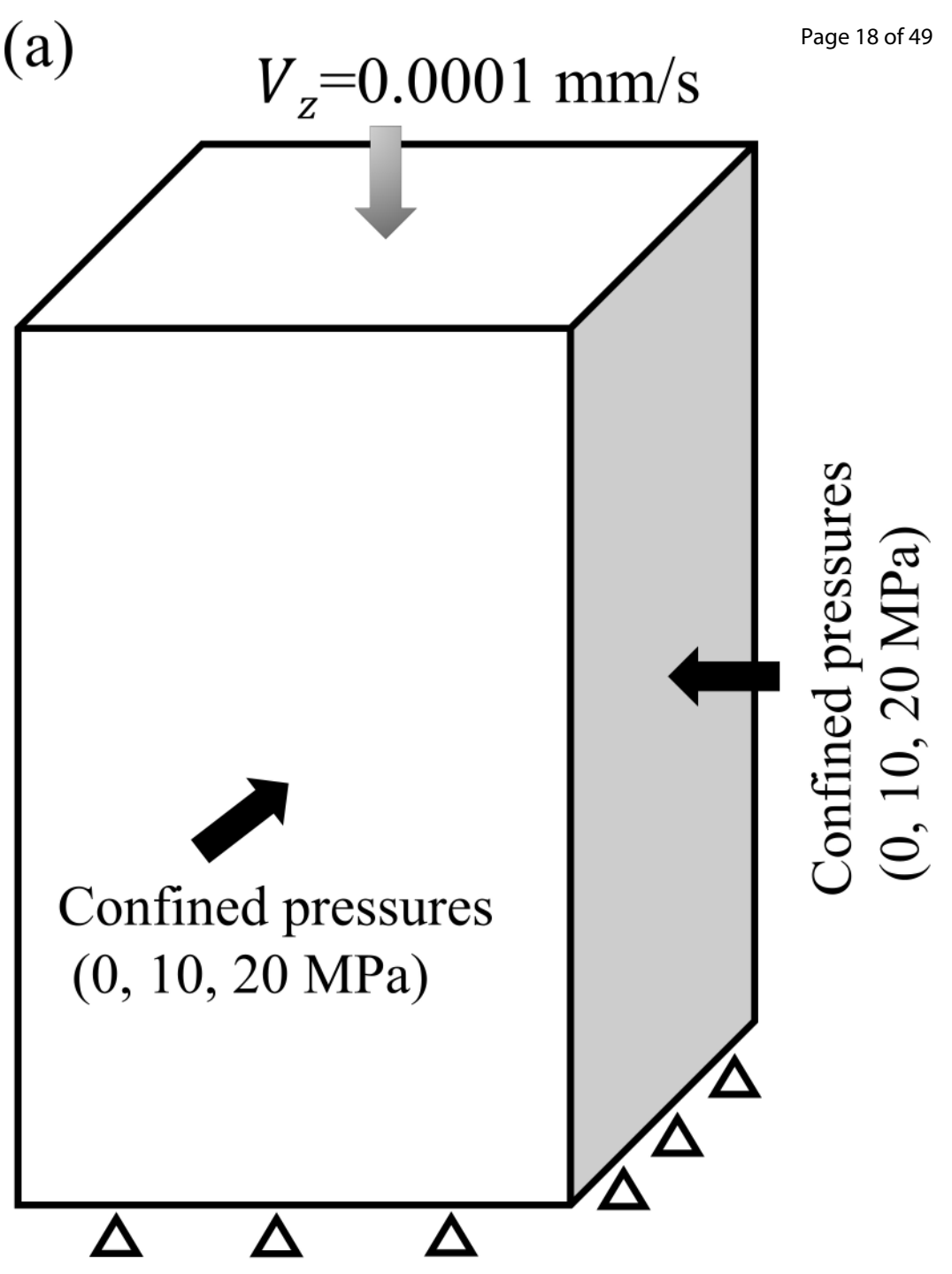
(a)
V_z=0.0001 mm/s
Confined pressures
(0, 10, 20 MPa)
Confined pressures
(0, 10, 20 MPa)

(b)

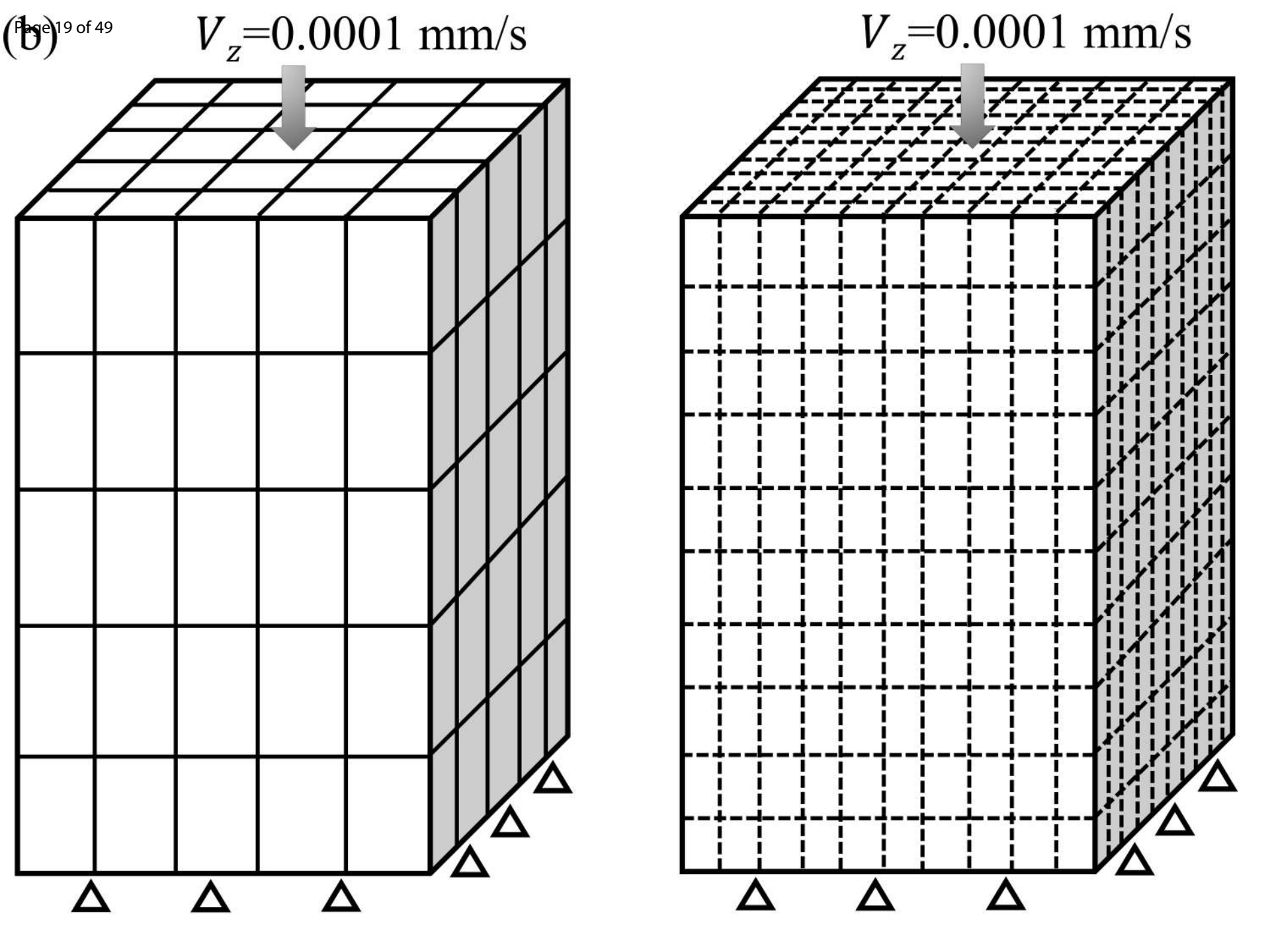

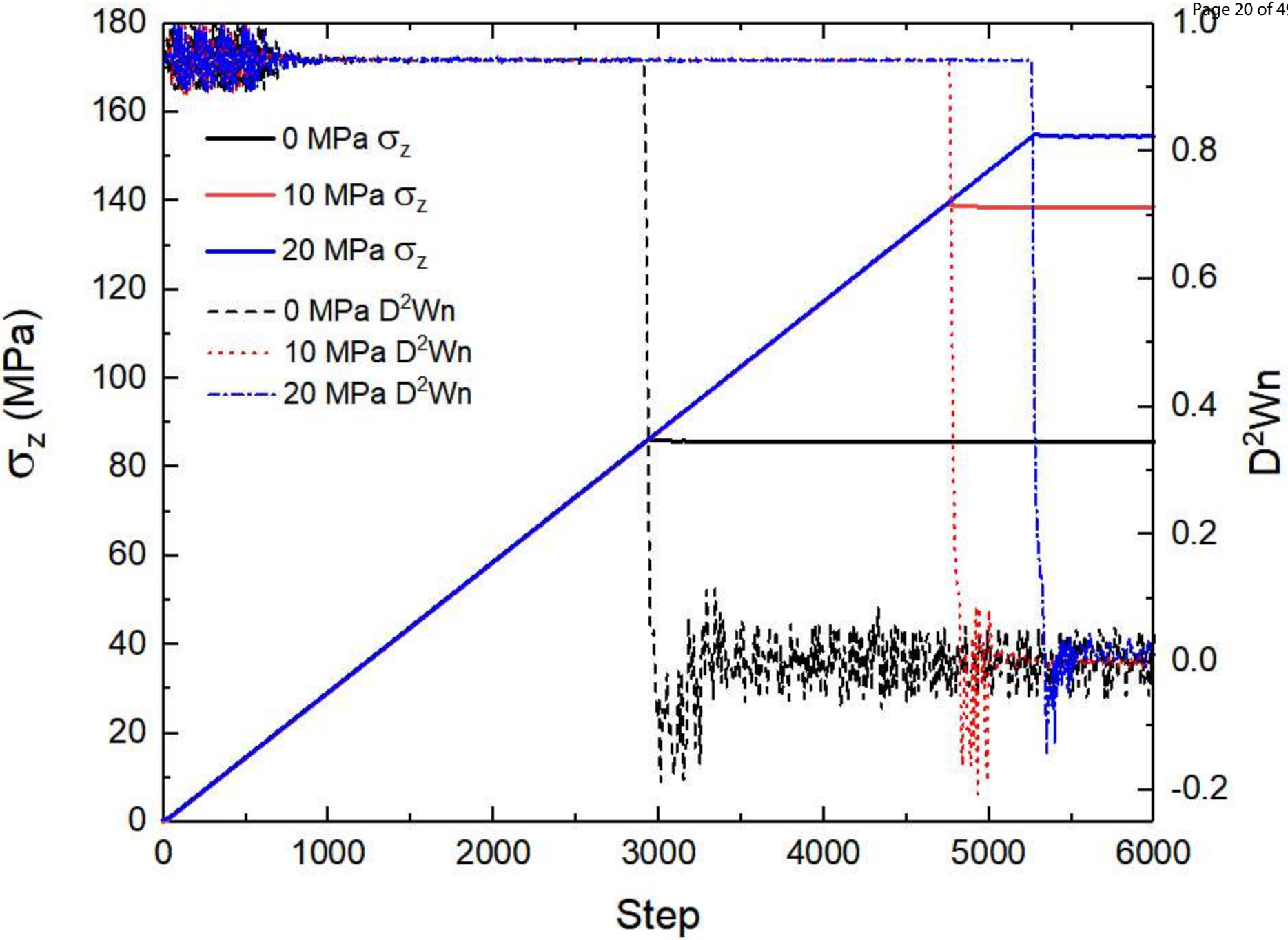
0 MPa σz
10 MPa σz
20 MPa σz
0 MPa D2Wn
10 MPa D2Wn
20 MPa D2Wn
σz (MPa)
D2Wn
Step
0
20
40
60
80
100
120
140
160
180
-0.2
0.0
0.2
0.4
0.6
0.8
1.0
0
1000
2000
3000
4000
5000
6000

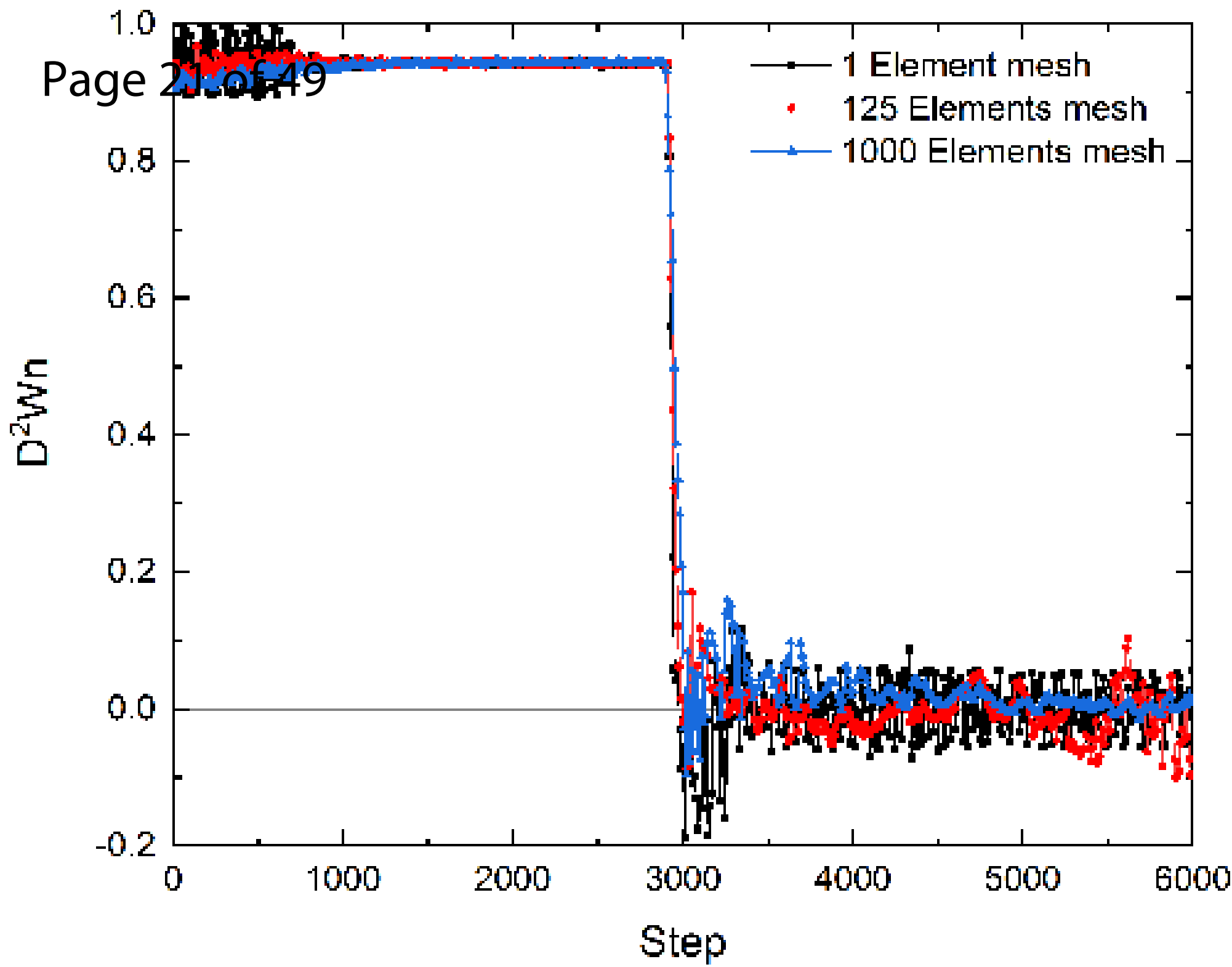
1 Element mesh
125 Elements mesh
1000 Elements mesh
D²Wn
Step
1.0
0.8
0.6
0.4
0.2
0.0
-0.2
0
1000
2000
3000
4000
5000
6000


Research area

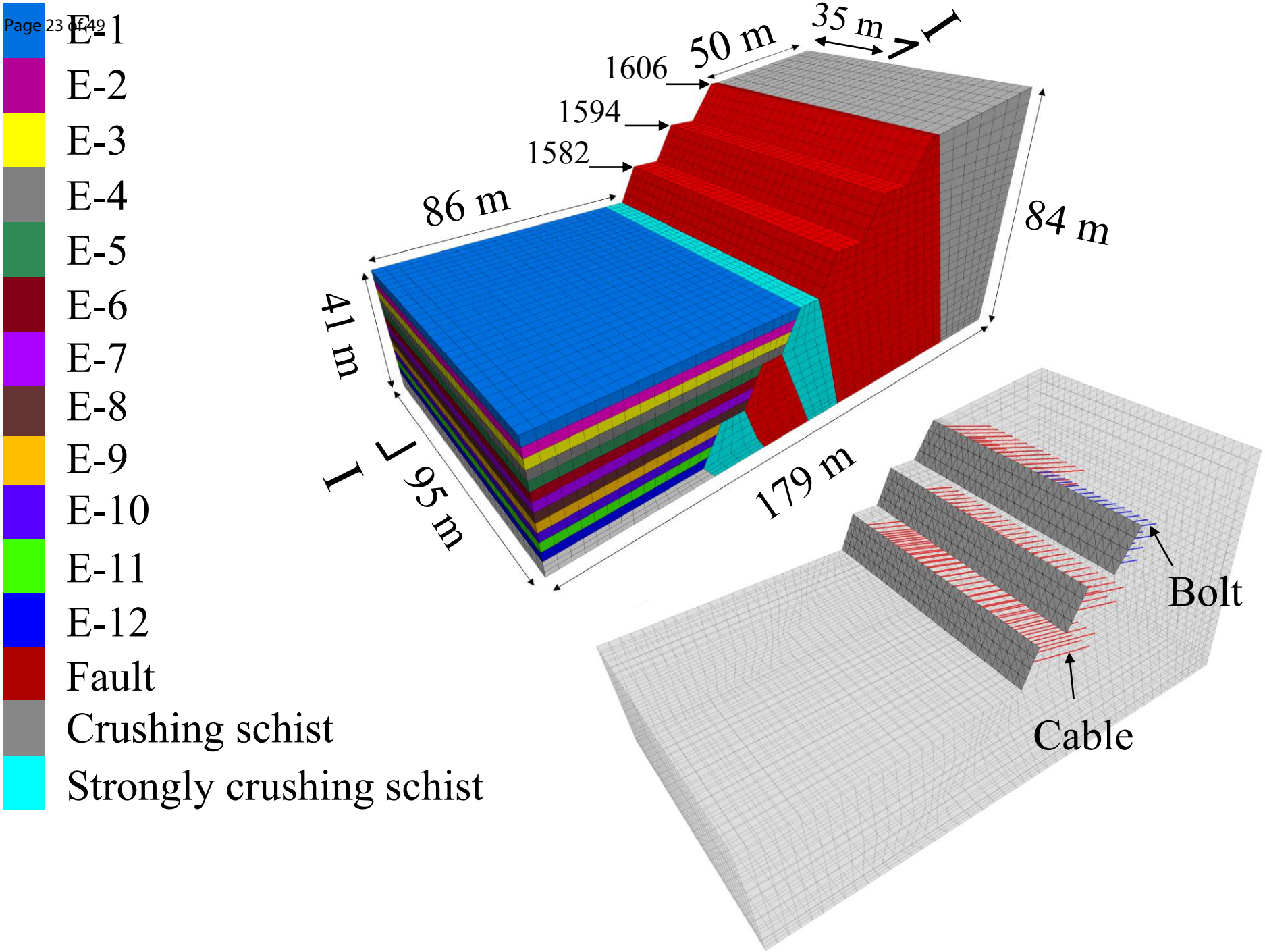
E-1
E-2
E-3
E-4
E-5
E-6
E-7
E-8
E-9
E-10
E-11
E-12
Fault
Crushing schist
Strongly crushing schist
1606
1594
1582
50 m
35 m
86 m
84 m
41 m
95 m
179 m
Bolt
Cable

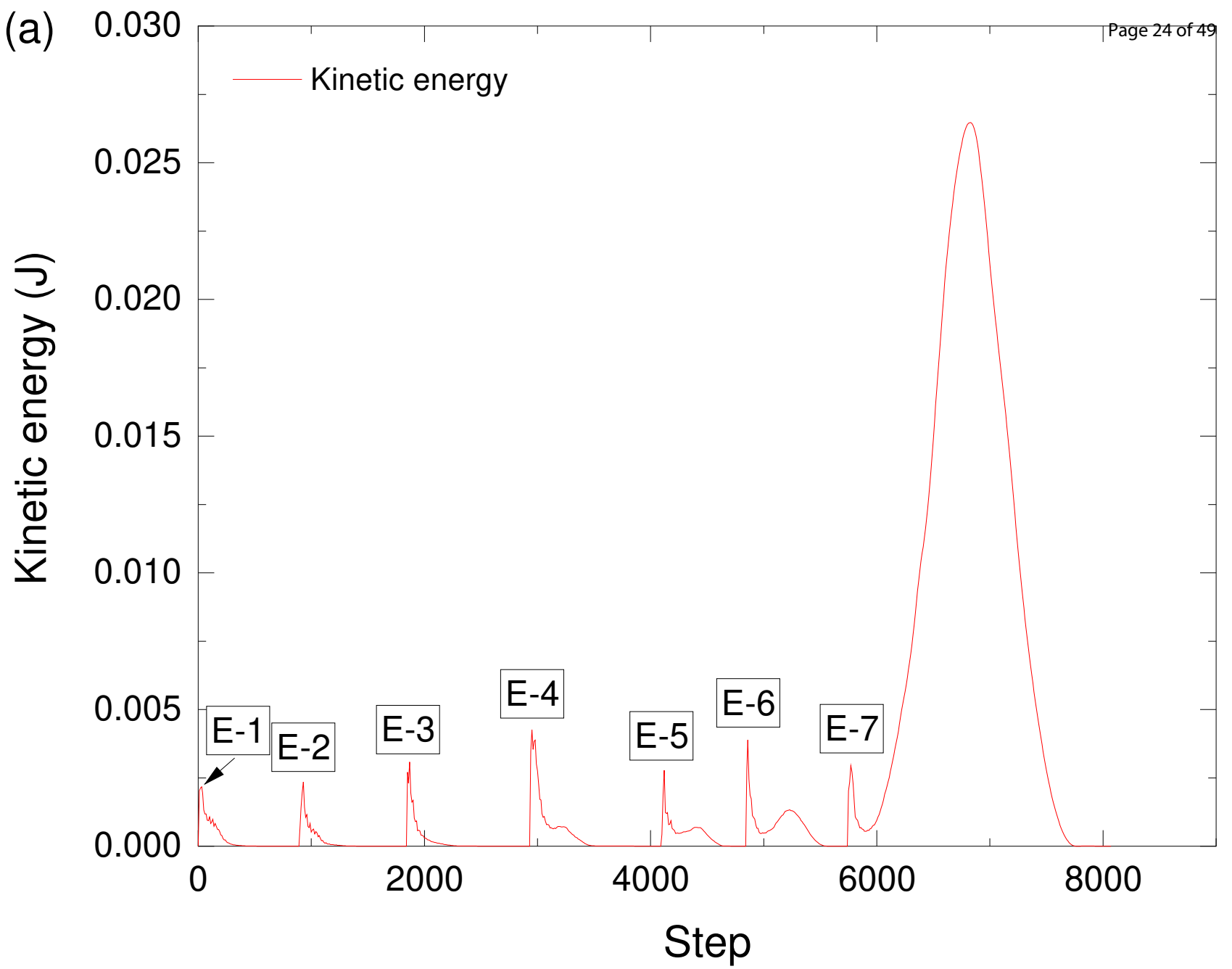
(a)
Kinetic energy
Kinetic energy (J)
0.030
0.025
0.020
0.015
0.010
0.005
0.000
E-1
E-2
E-3
E-4
E-5
E-6
E-7
0
2000
4000
6000
8000
Step

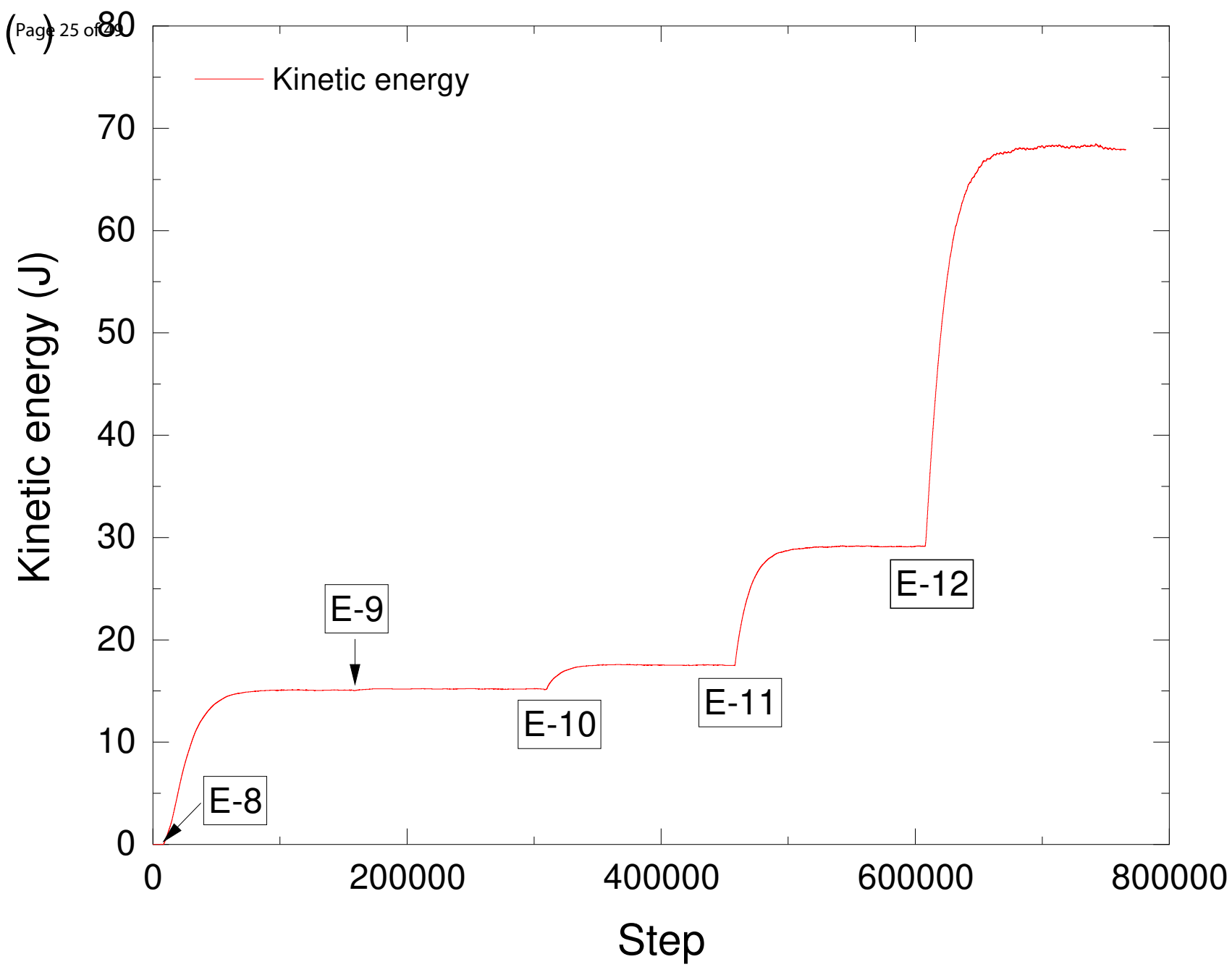
Kinetic energy
Kinetic energy (J)
Step
0
10
20
30
40
50
60
70
80
0
200000
400000
600000
800000
E-8
E-9
E-10
E-11
E-12

( )

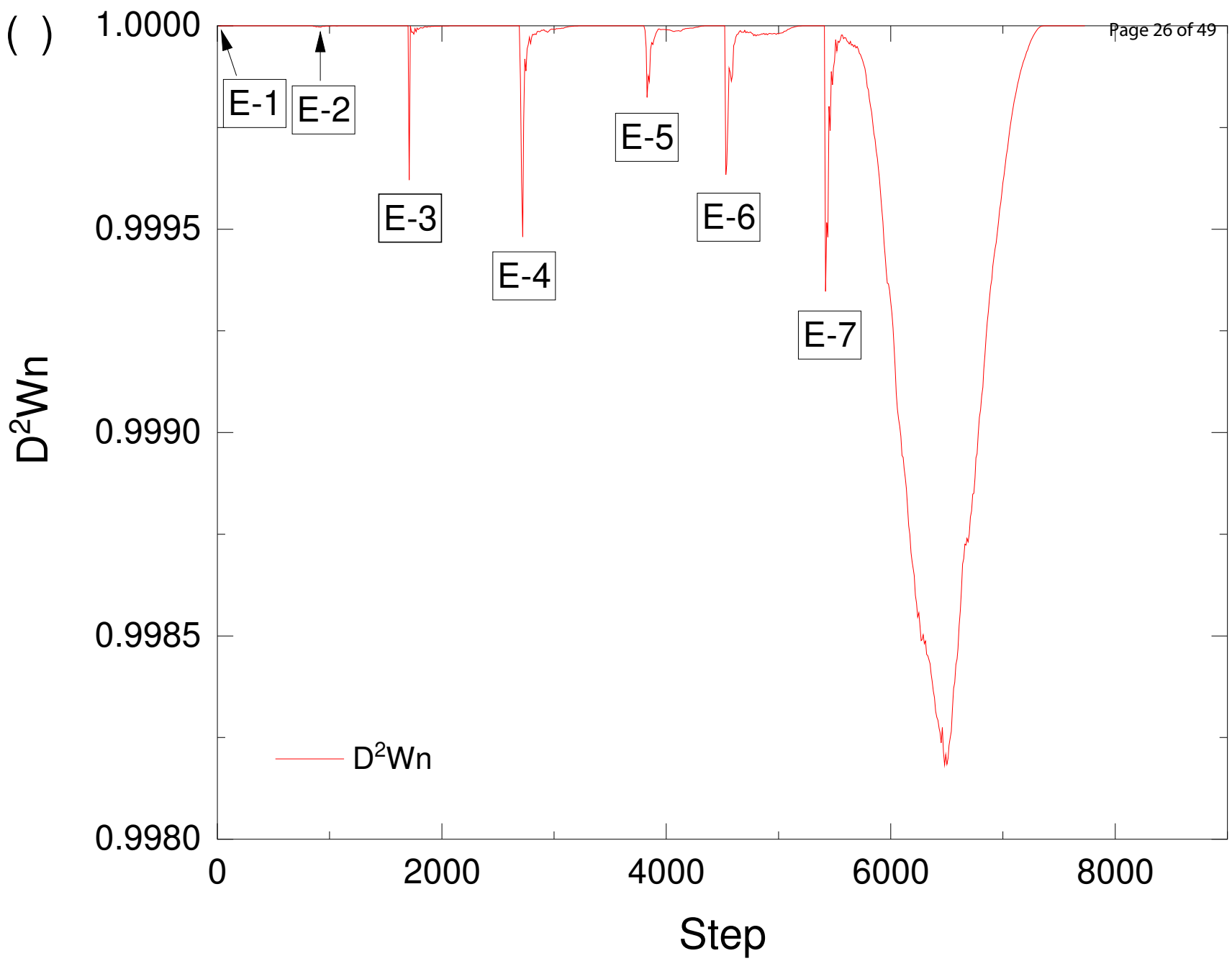
1.0000
0.9995
0.9990
0.9985
0.9980
D²Wn
0
2000
4000
6000
8000
Step
E-1
E-2
E-3
E-4
E-5
E-6
E-7
D²Wn

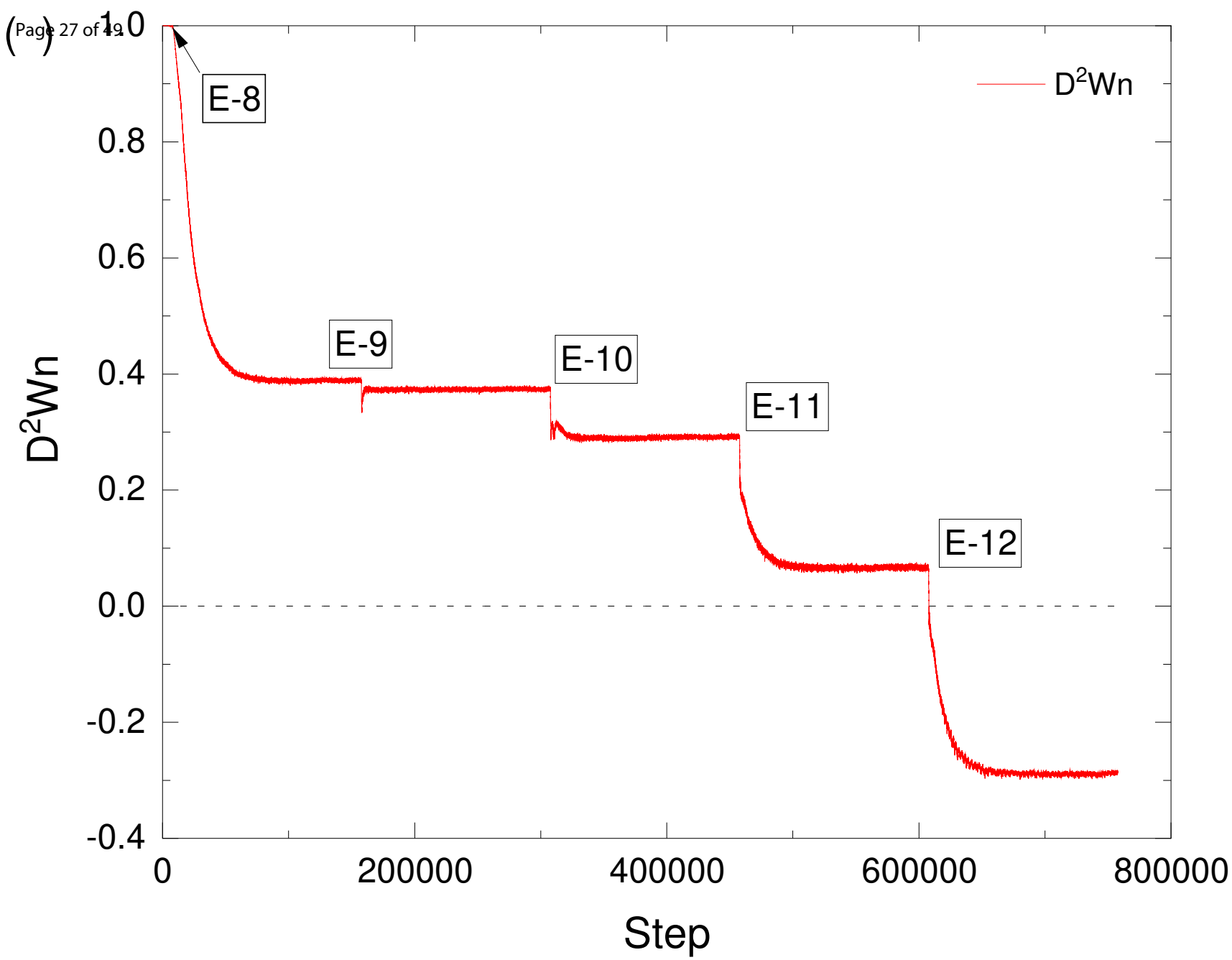
E-8
E-9
E-10
E-11
E-12
D²Wn
D²Wn
Step
1.0
0.8
0.6
0.4
0.2
0.0
-0.2
-0.4
0
200000
400000
600000
800000

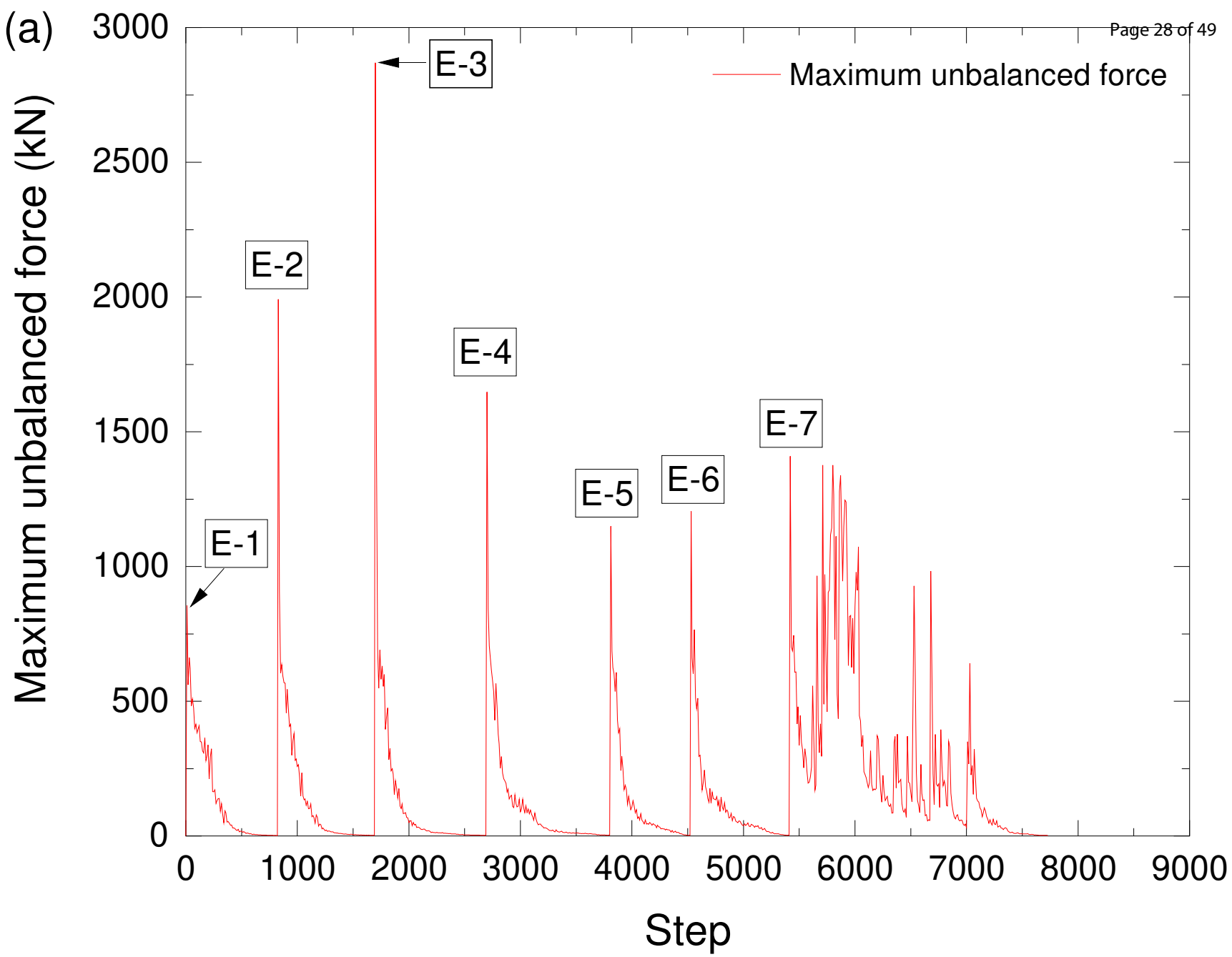
(a)
Maximum unbalanced force (kN)
3000
2500
2000
1500
1000
500
0
0
1000
2000
3000
4000
5000
6000
7000
8000
9000
Step
Maximum unbalanced force
E-1
E-2
E-3
E-4
E-5
E-6
E-7

(b)

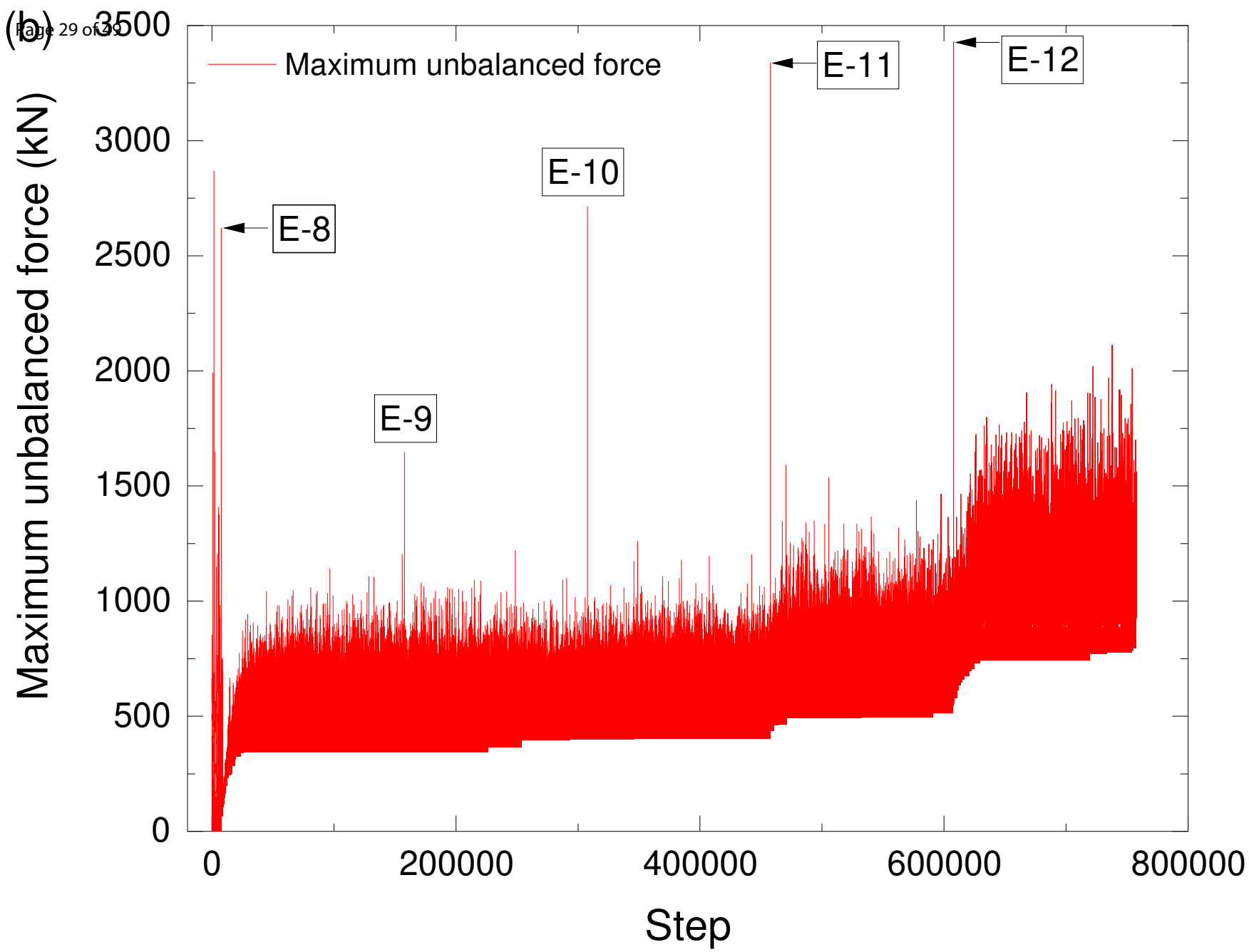
Maximum unbalanced force
E-8
E-9
E-10
E-11
E-12
Maximum unbalanced force (kN)
Step
0
500
1000
1500
2000
2500
3000
3500
0
200000
400000
600000
800000

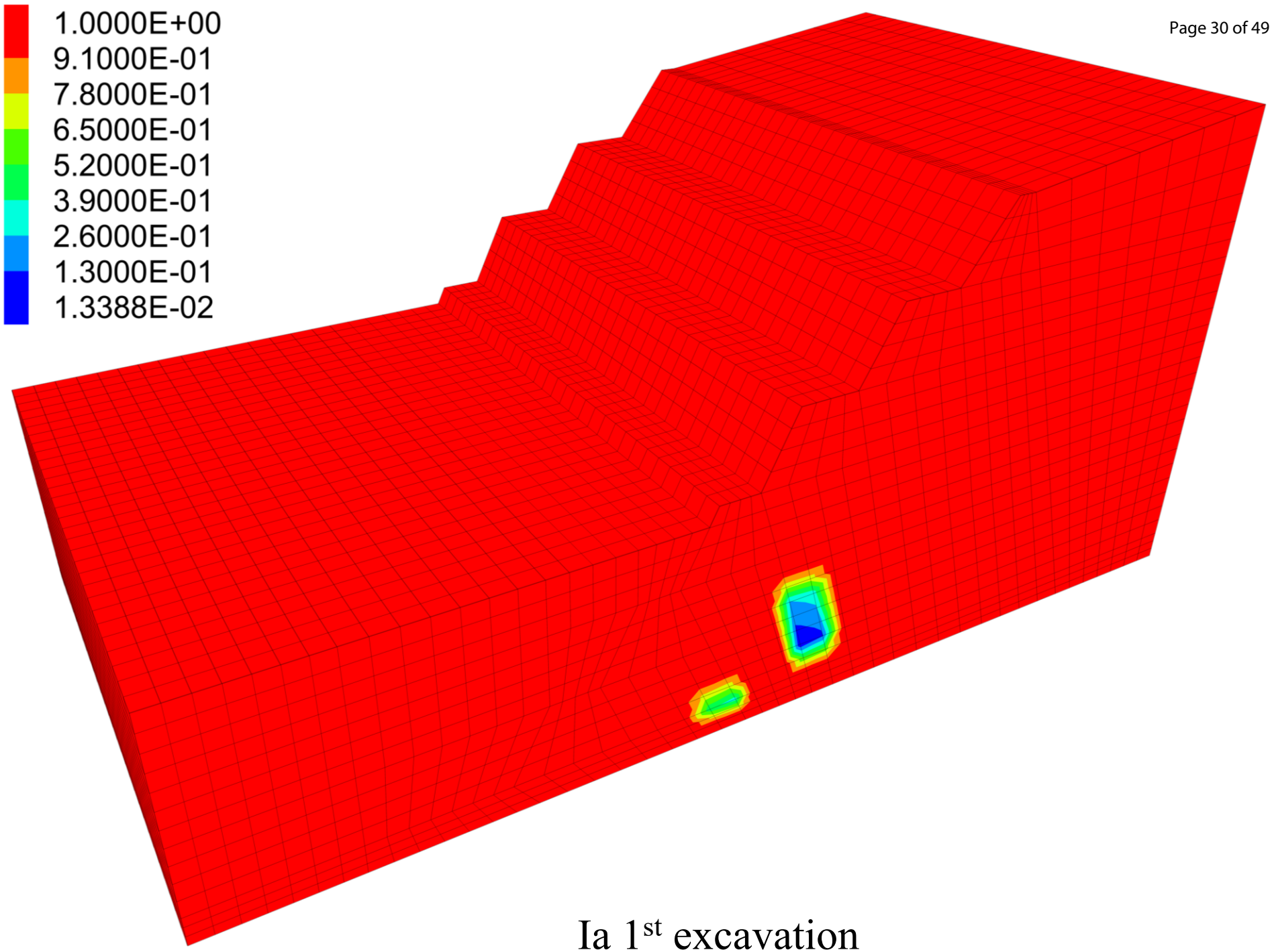

Ia 1st excavation

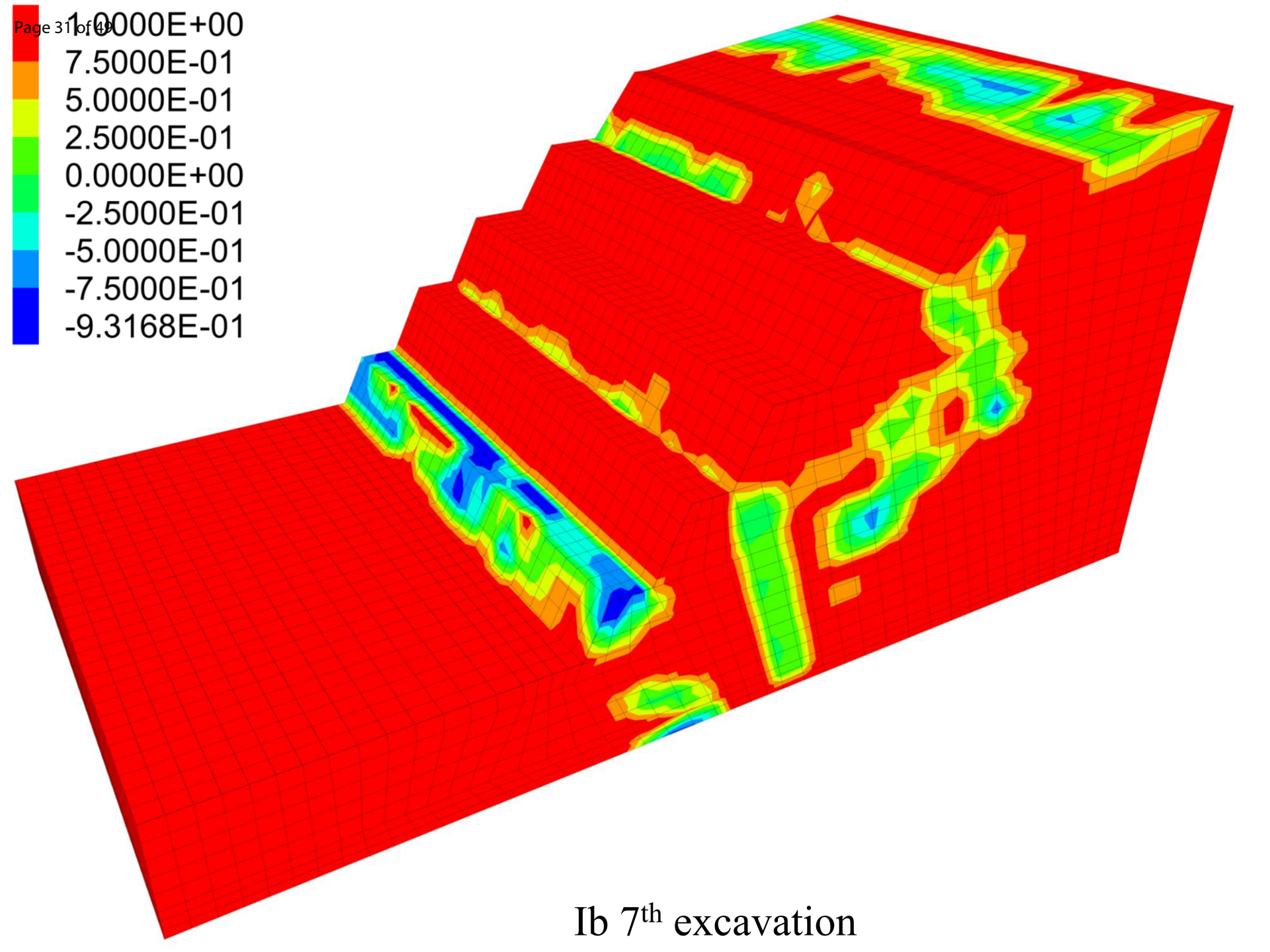

Ib 7th excavation

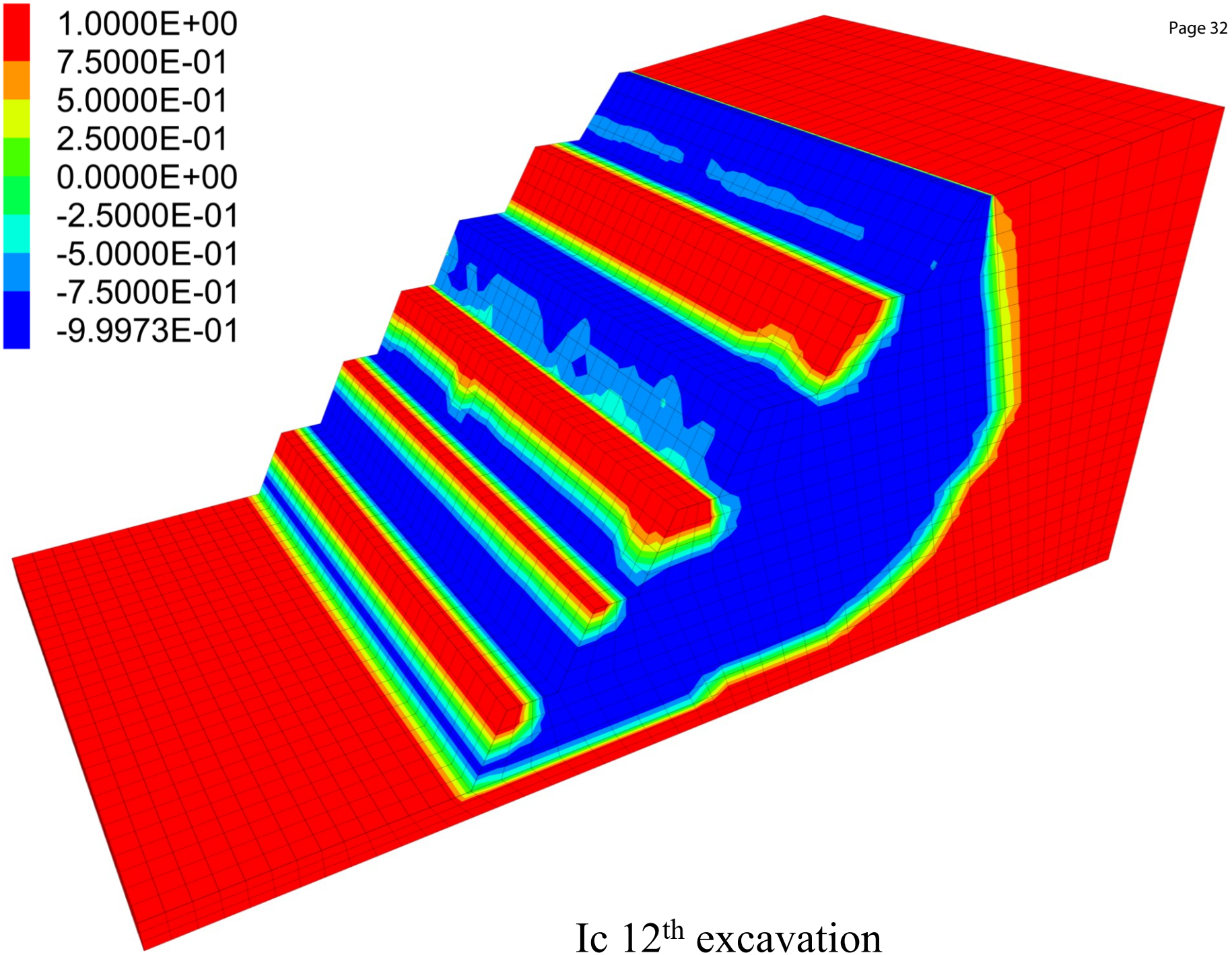

Ic 12th excavation

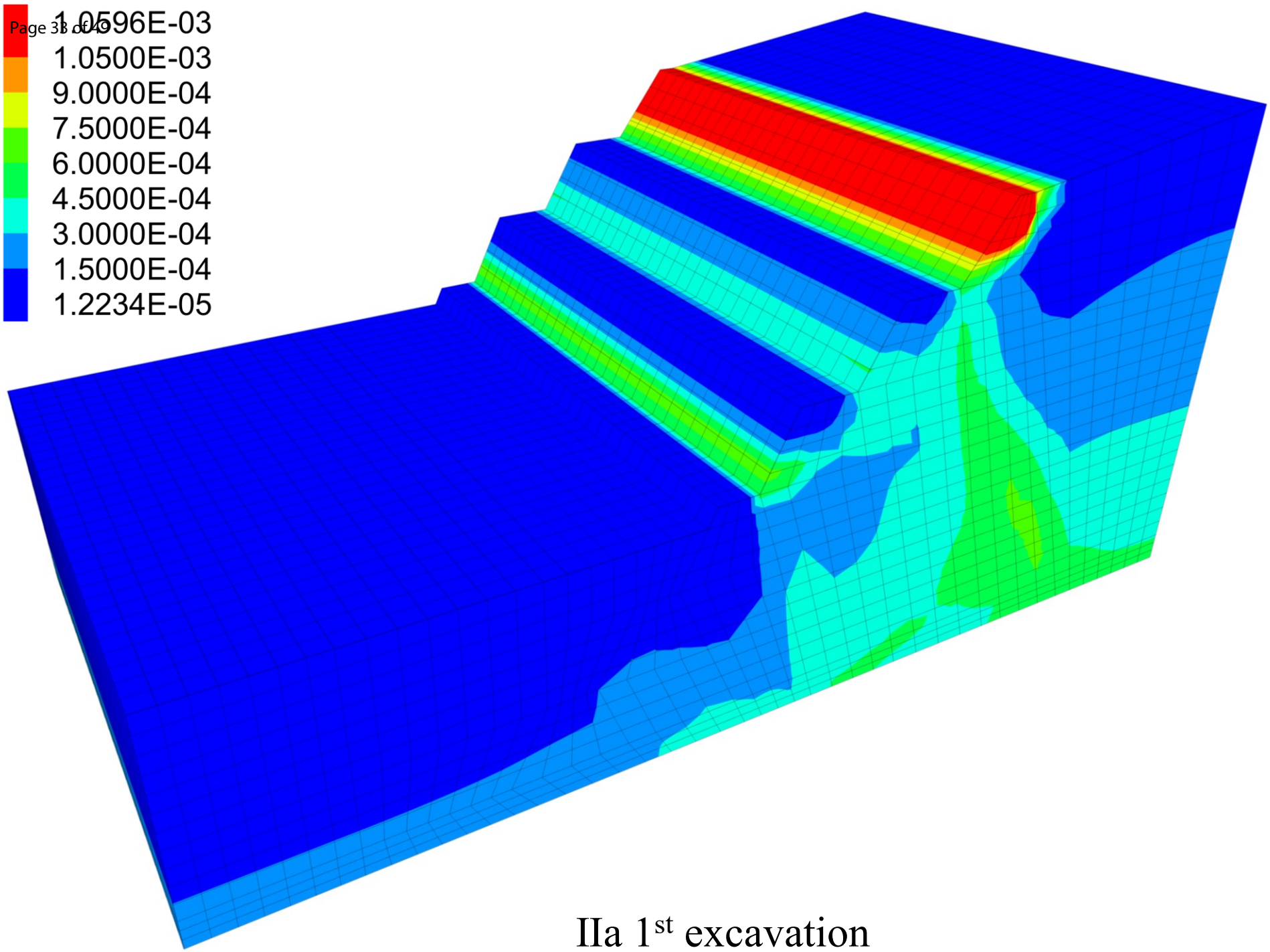

IIa 1st excavation

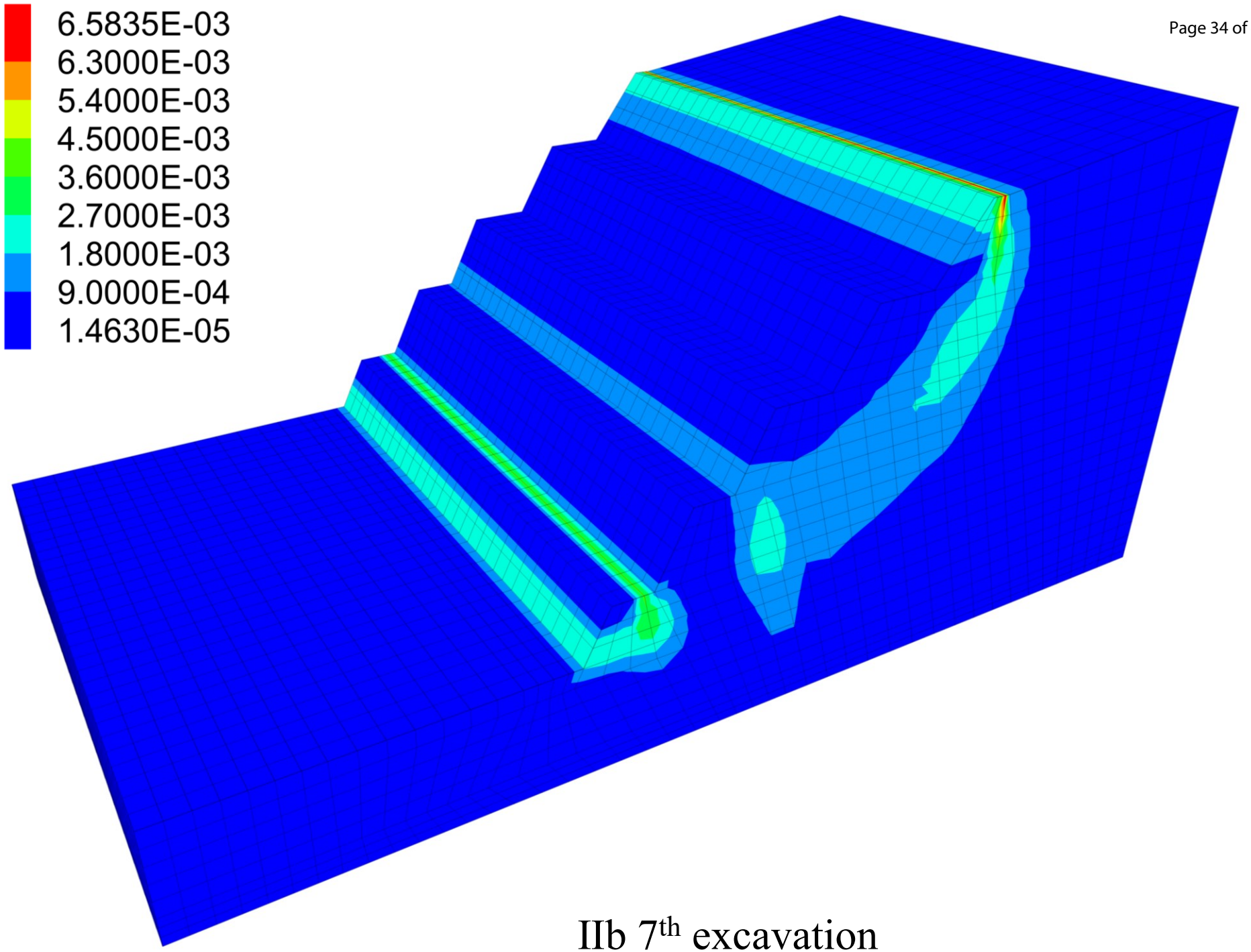

IIb 7th excavation

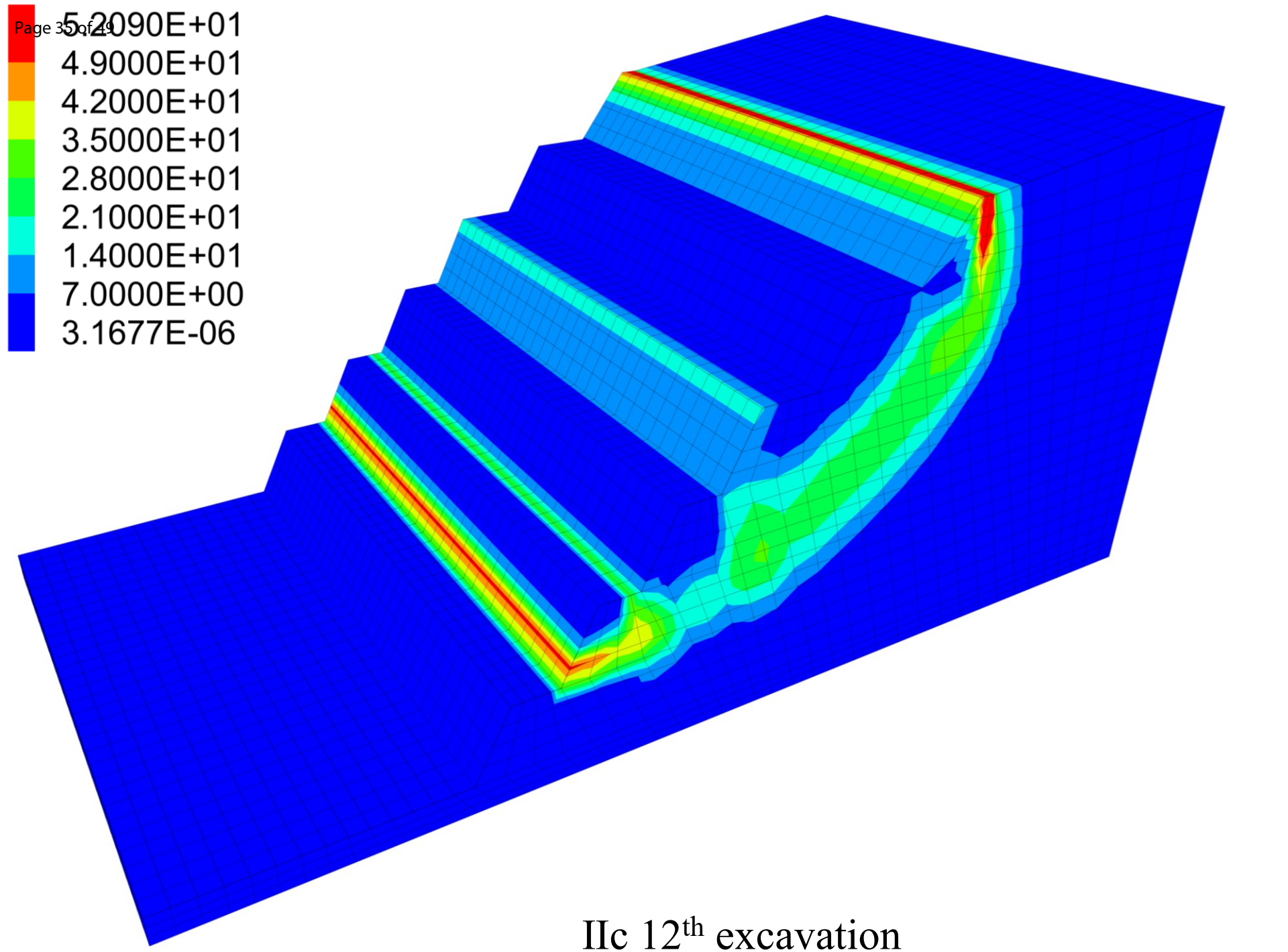

IIc 12th excavation

(a)

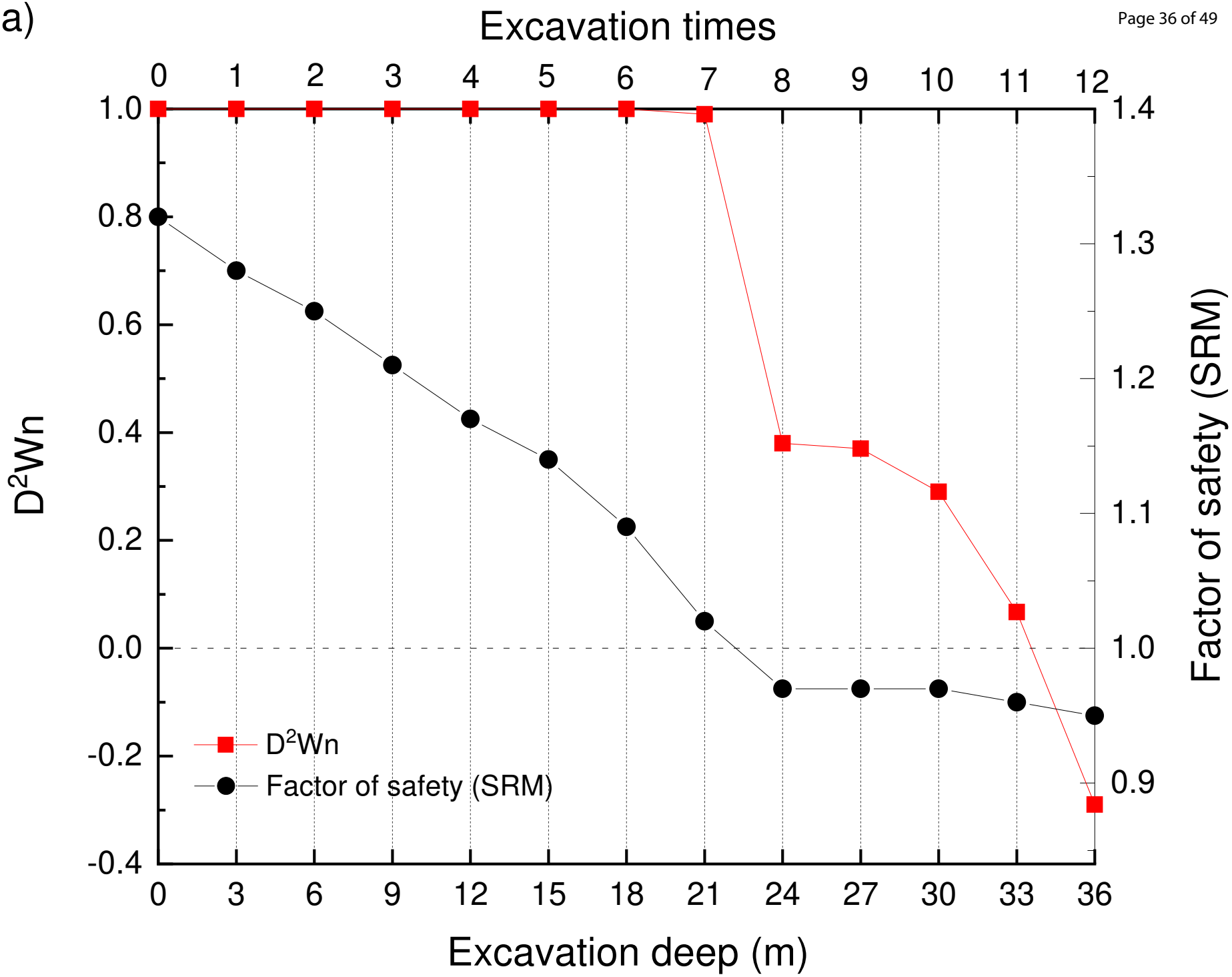
Excavation times
0
1
2
3
4
5
6
7
8
9
10
11
12
1.0
0.8
0.6
0.4
0.2
0.0
-0.2
-0.4
D²Wn
1.4
1.3
1.2
1.1
1.0
0.9
Factor of safety (SRM)
D²Wn
Factor of safety (SRM)
0
3
6
9
12
15
18
21
24
27
30
33
36
Excavation deep (m)

(b)

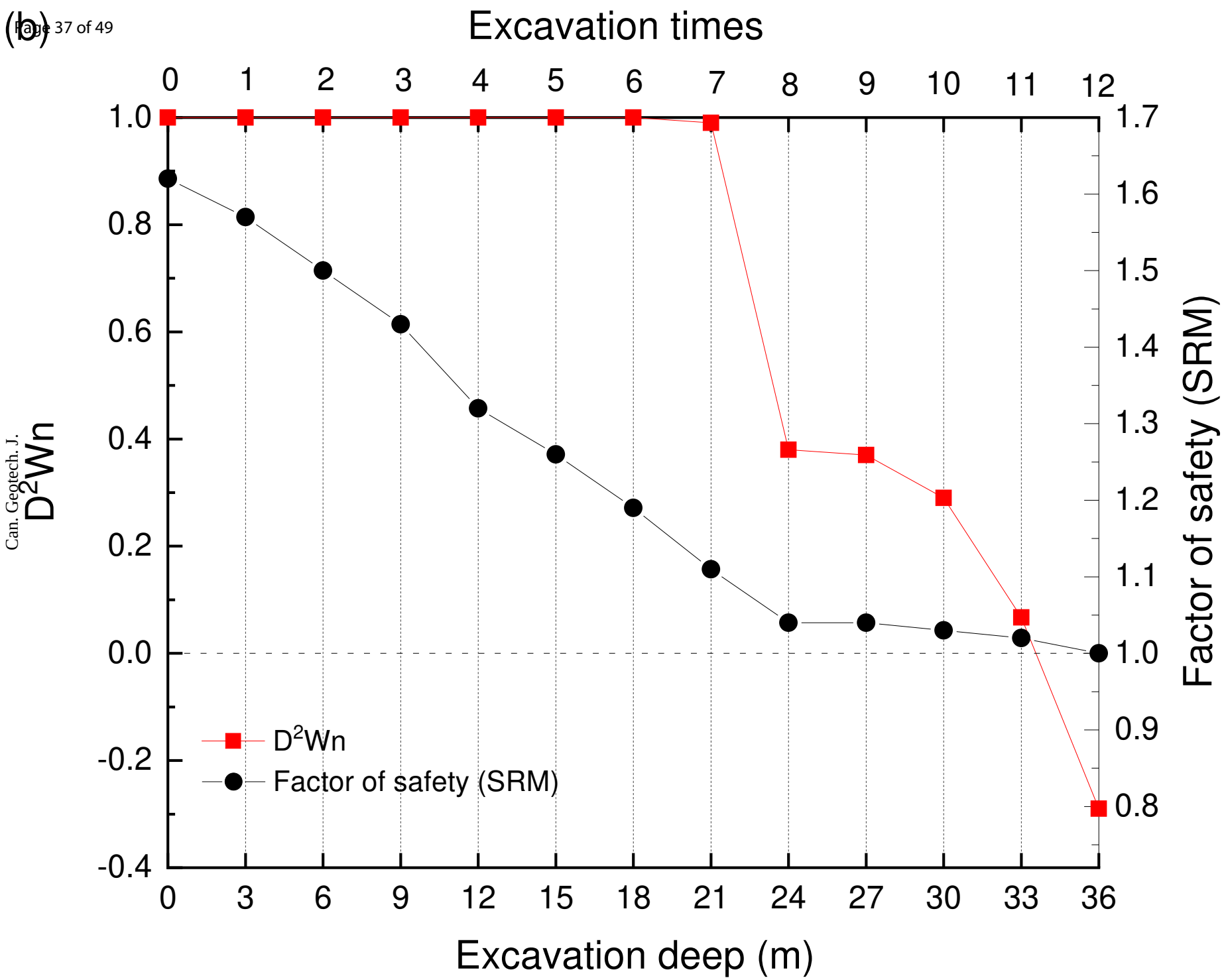

Can. Geotech. J.

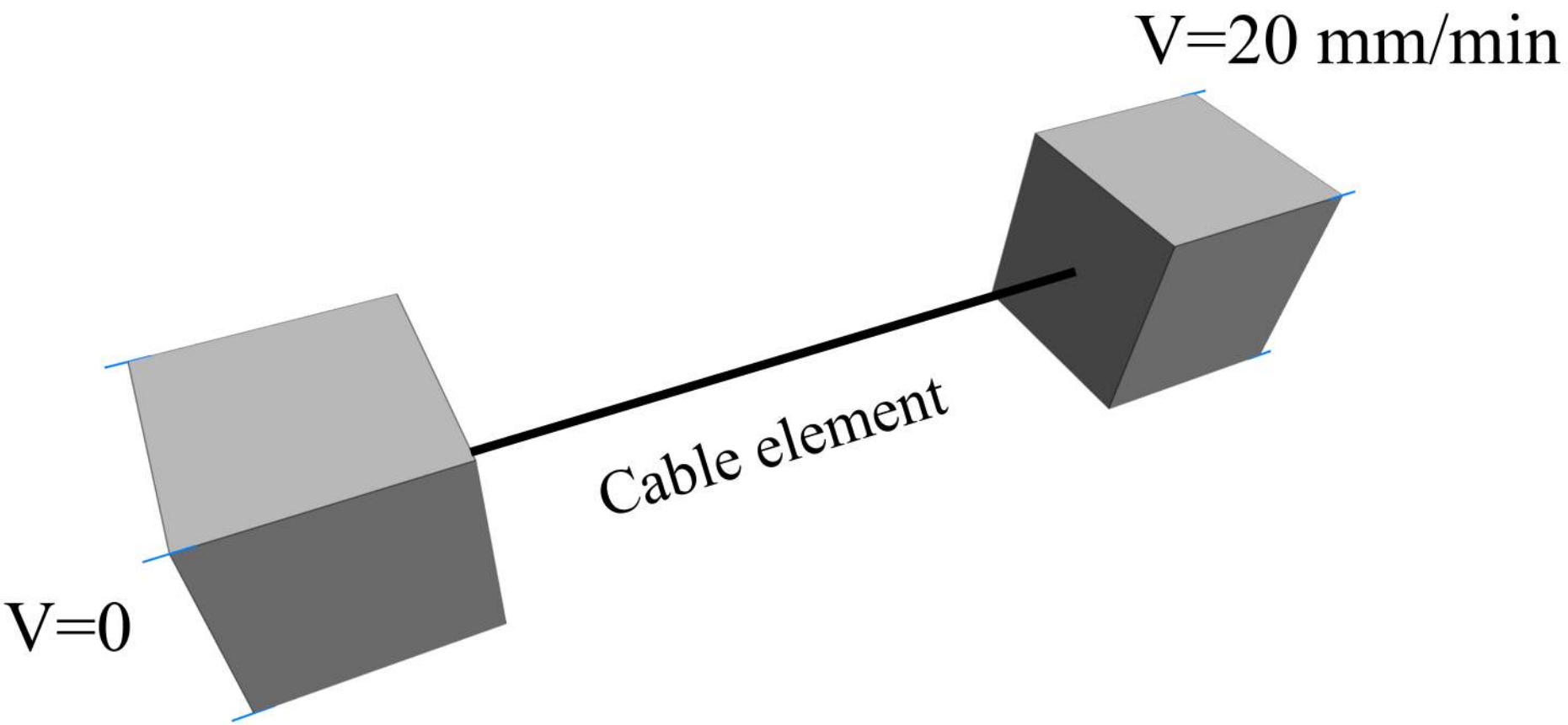
V=20 mm/min
Cable element
V=0

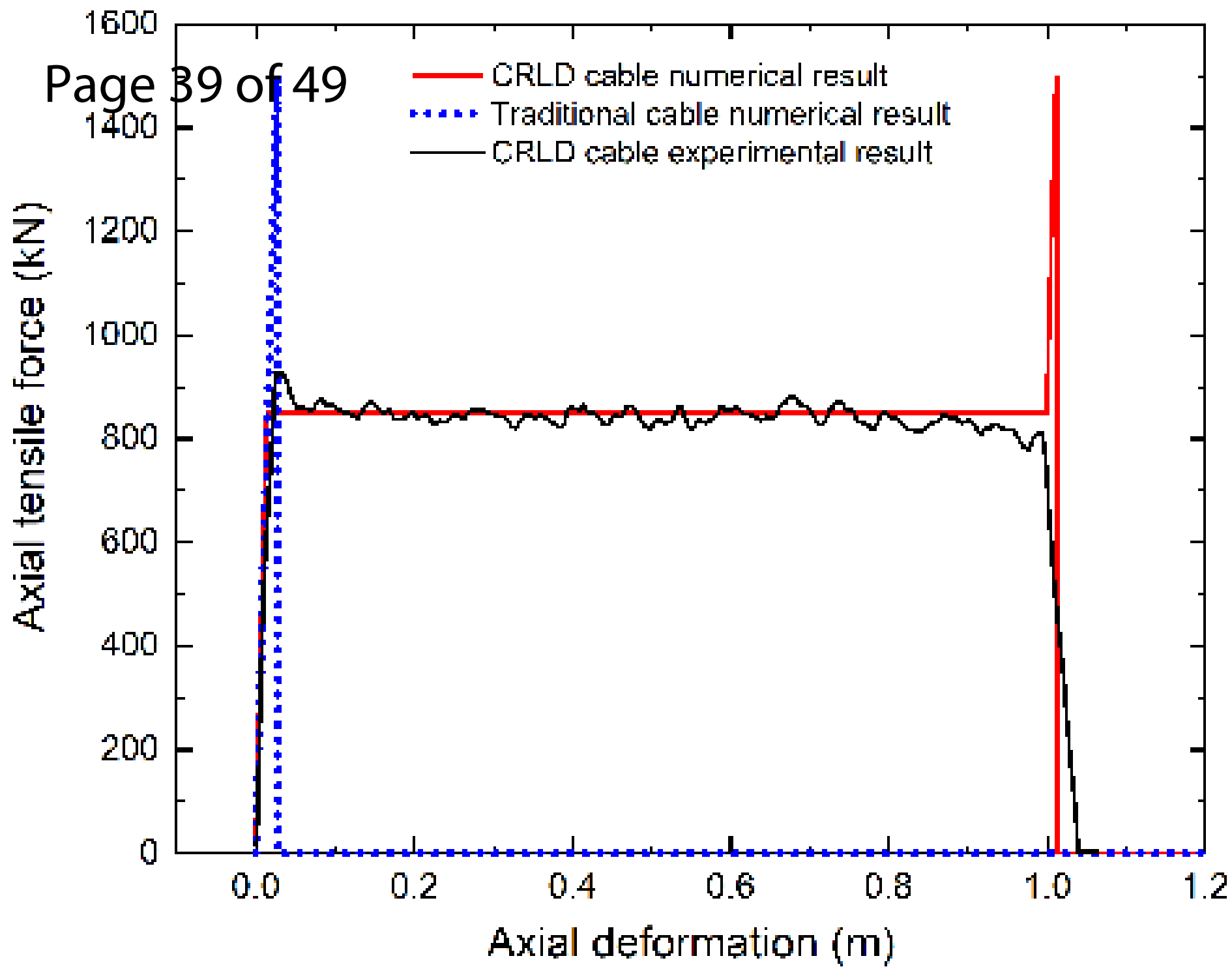
CRLD cable numerical result
Traditional cable numerical result
CRLD cable experimental result
Axial tensile force (kN)
Axial deformation (m)
0
200
400
600
800
1000
1200
1400
1600
0.0
0.2
0.4
0.6
0.8
1.0
1.2

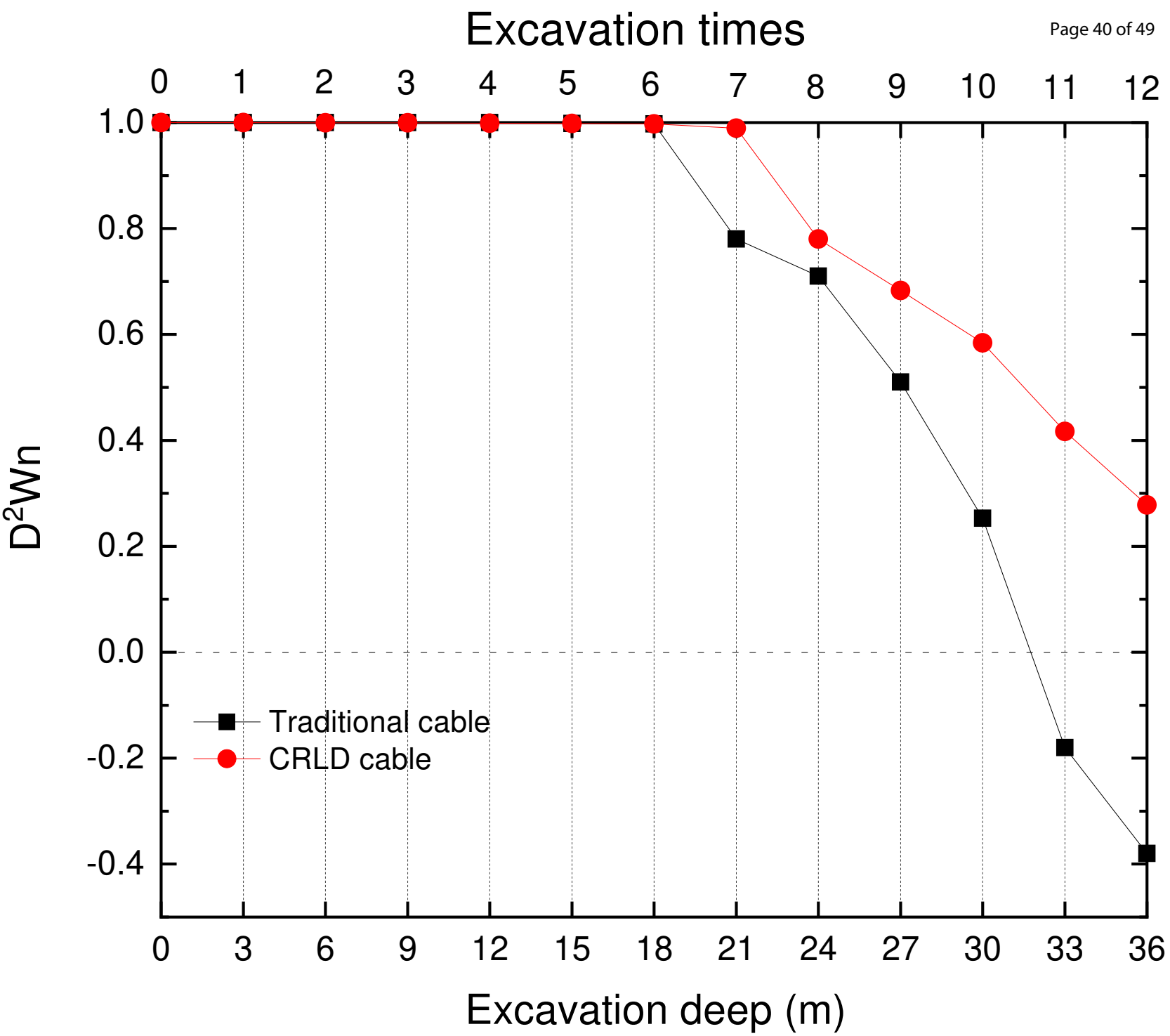
Excavation times
0
1
2
3
4
5
6
7
8
9
10
11
12
1.0
0.8
0.6
0.4
0.2
0.0
-0.2
-0.4
D²Wn
Traditional cable
CRLD cable
0
3
6
9
12
15
18
21
24
27
30
33
36
Excavation deep (m)

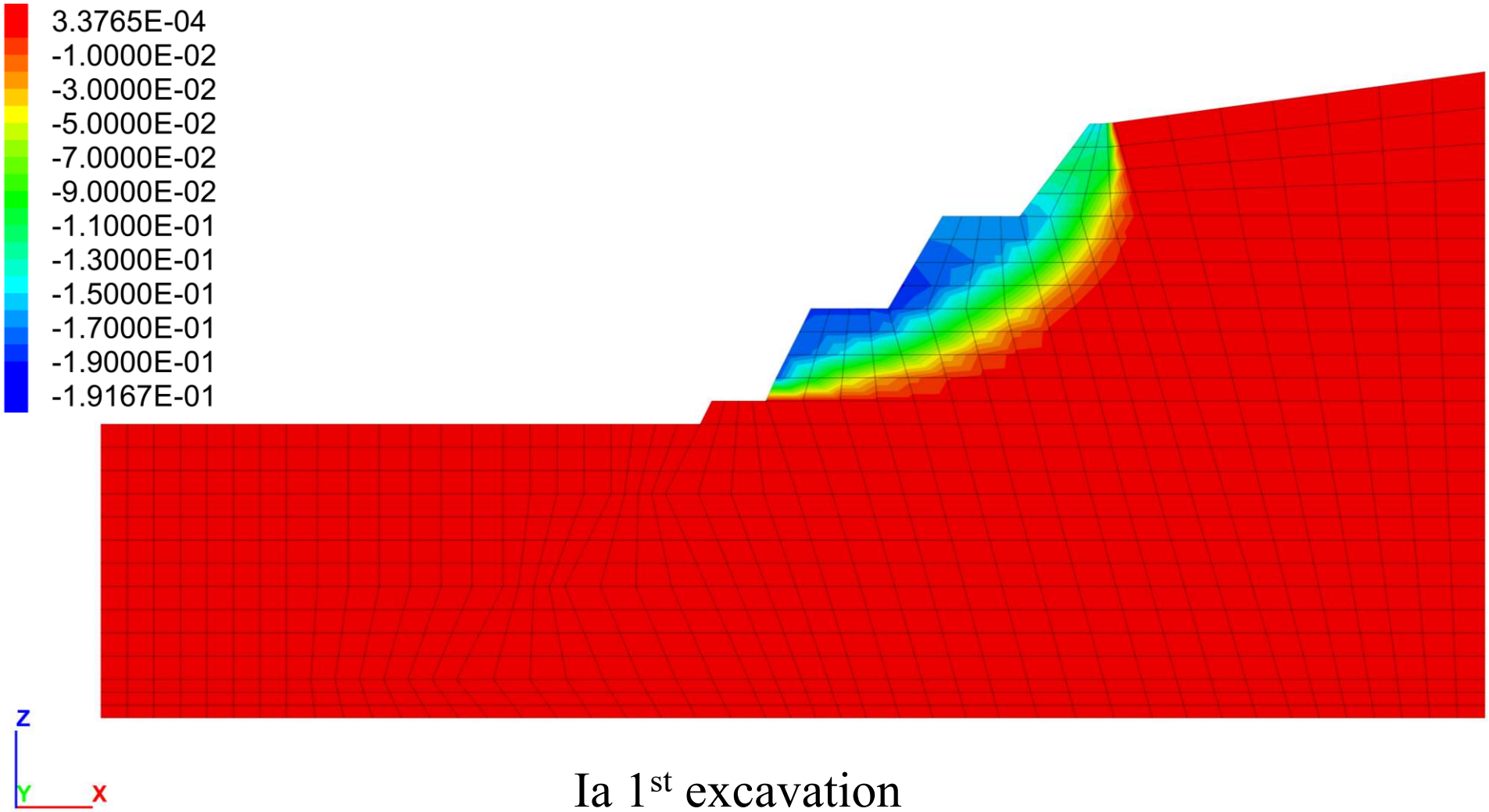

Ia 1st excavation

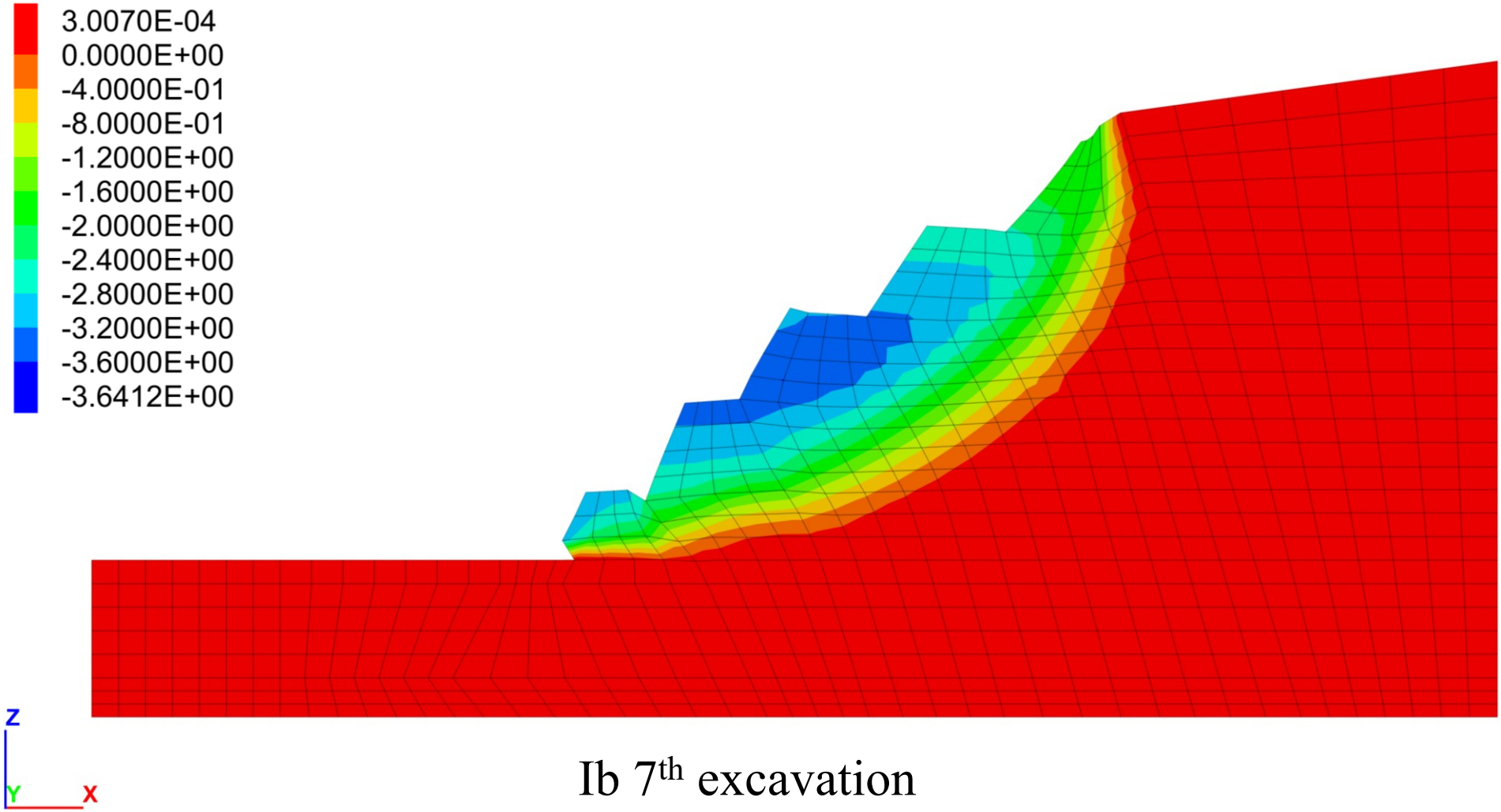

Ib 7th excavation

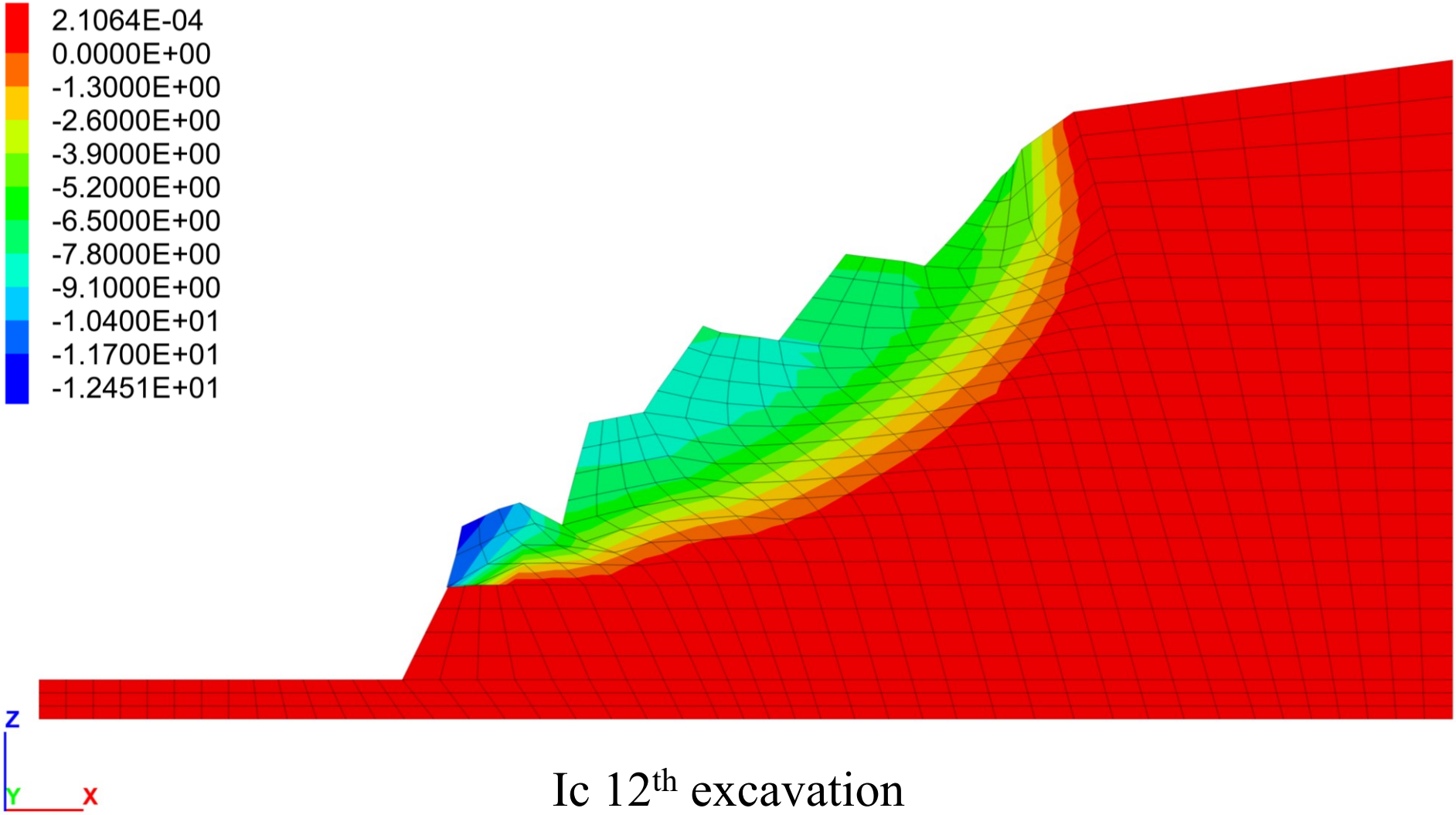

Ic 12th excavation

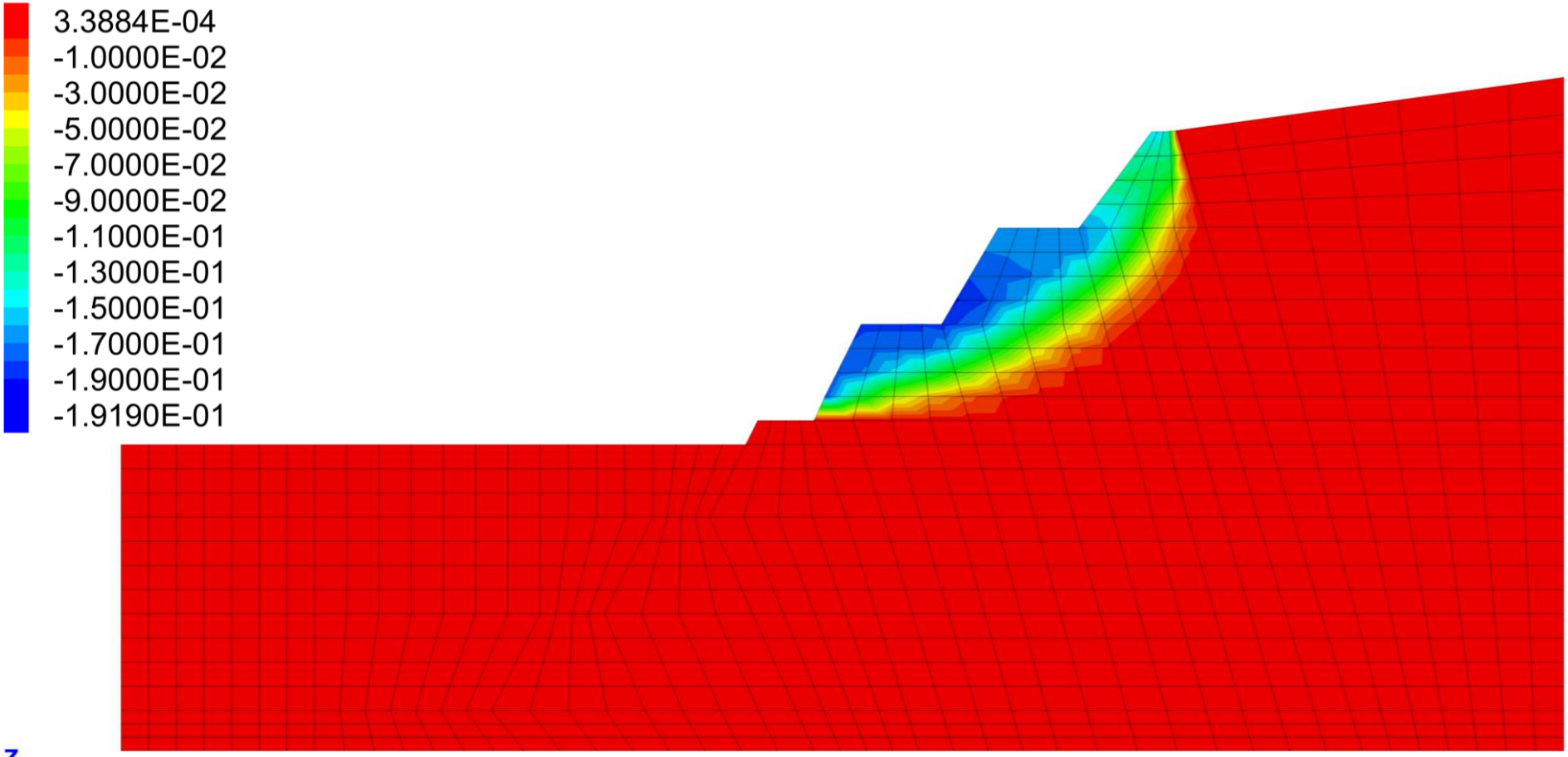

IIa 1st excavation

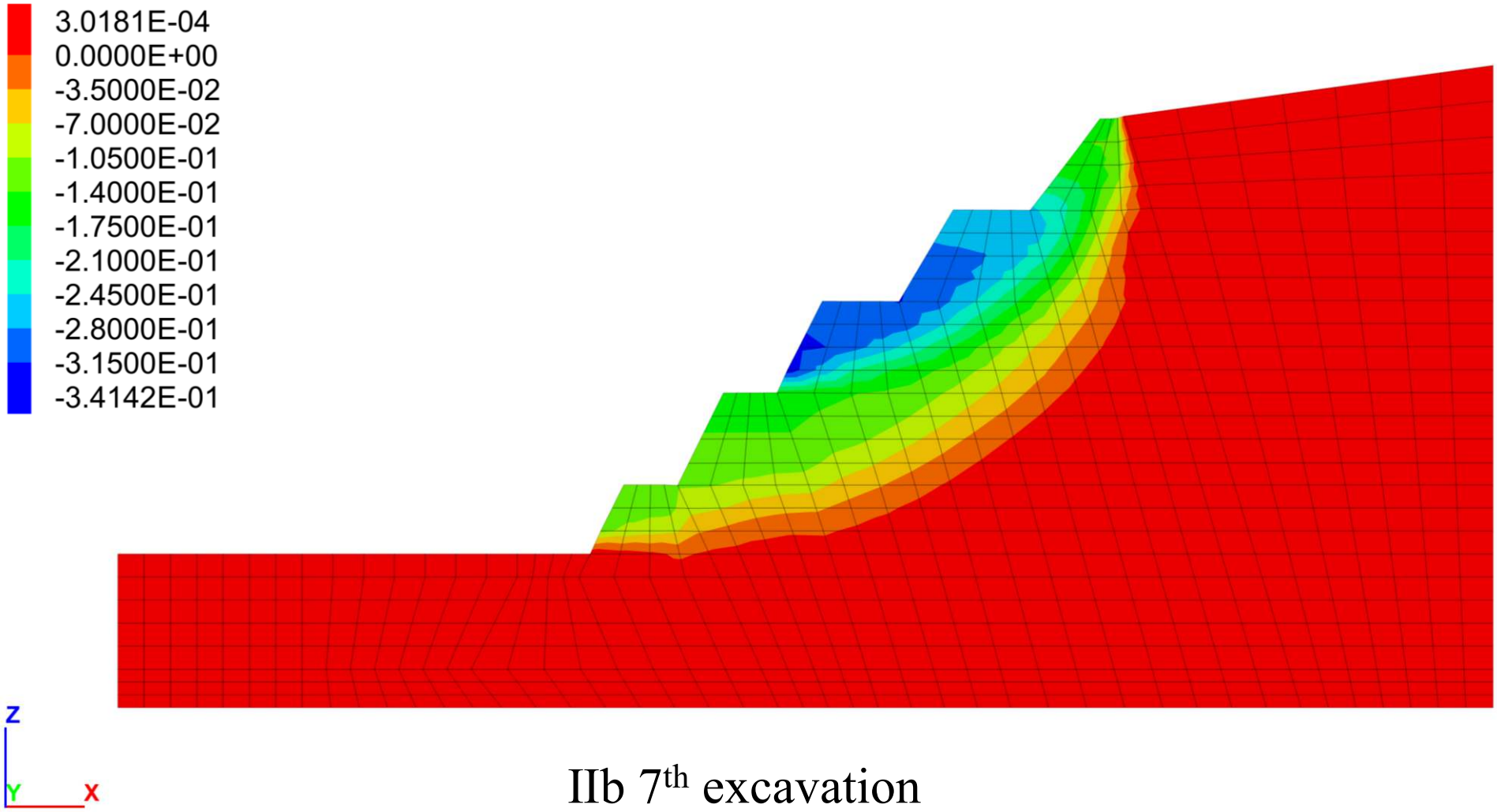

IIb 7th excavation

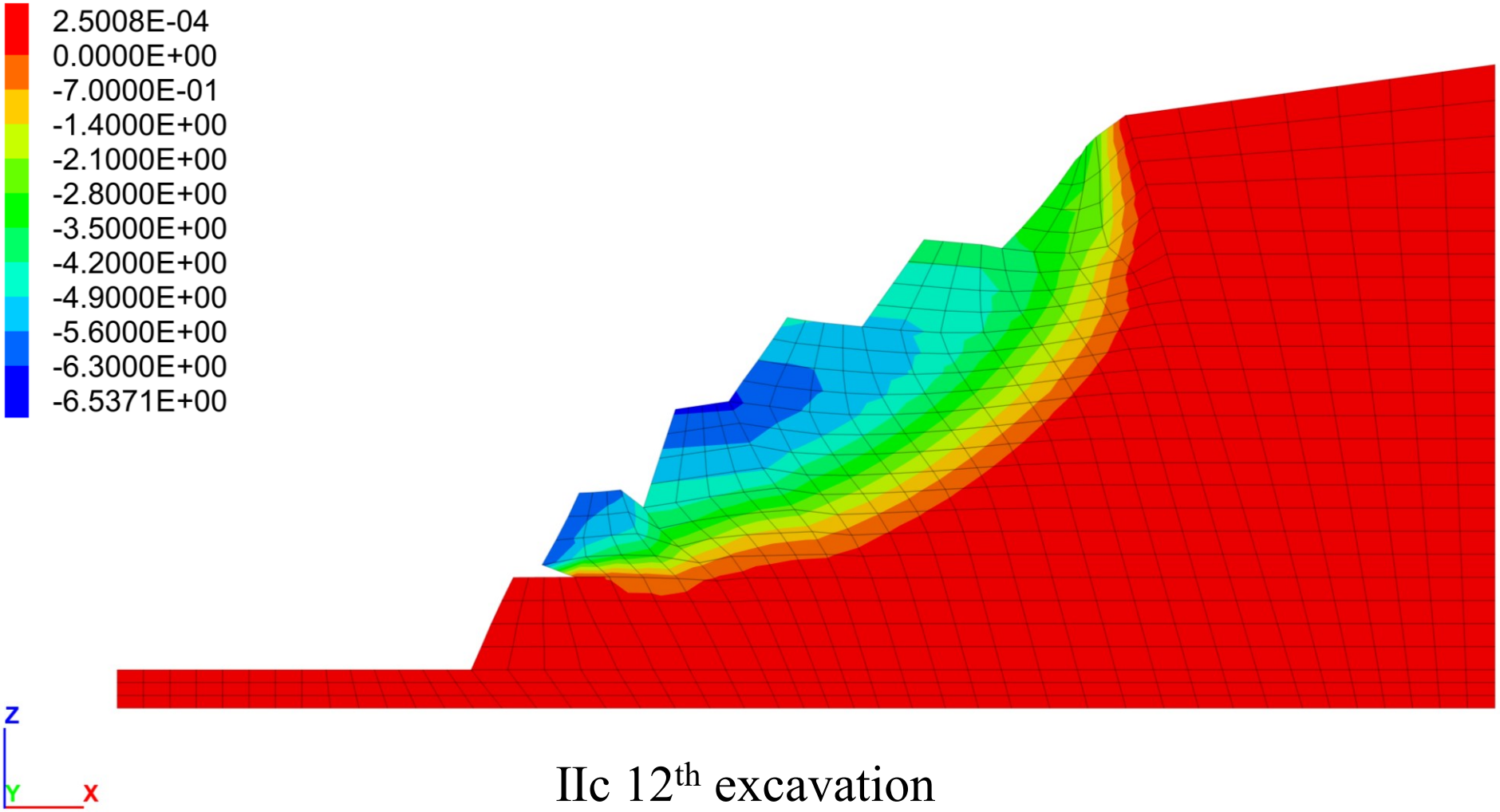

IIc 12th excavation

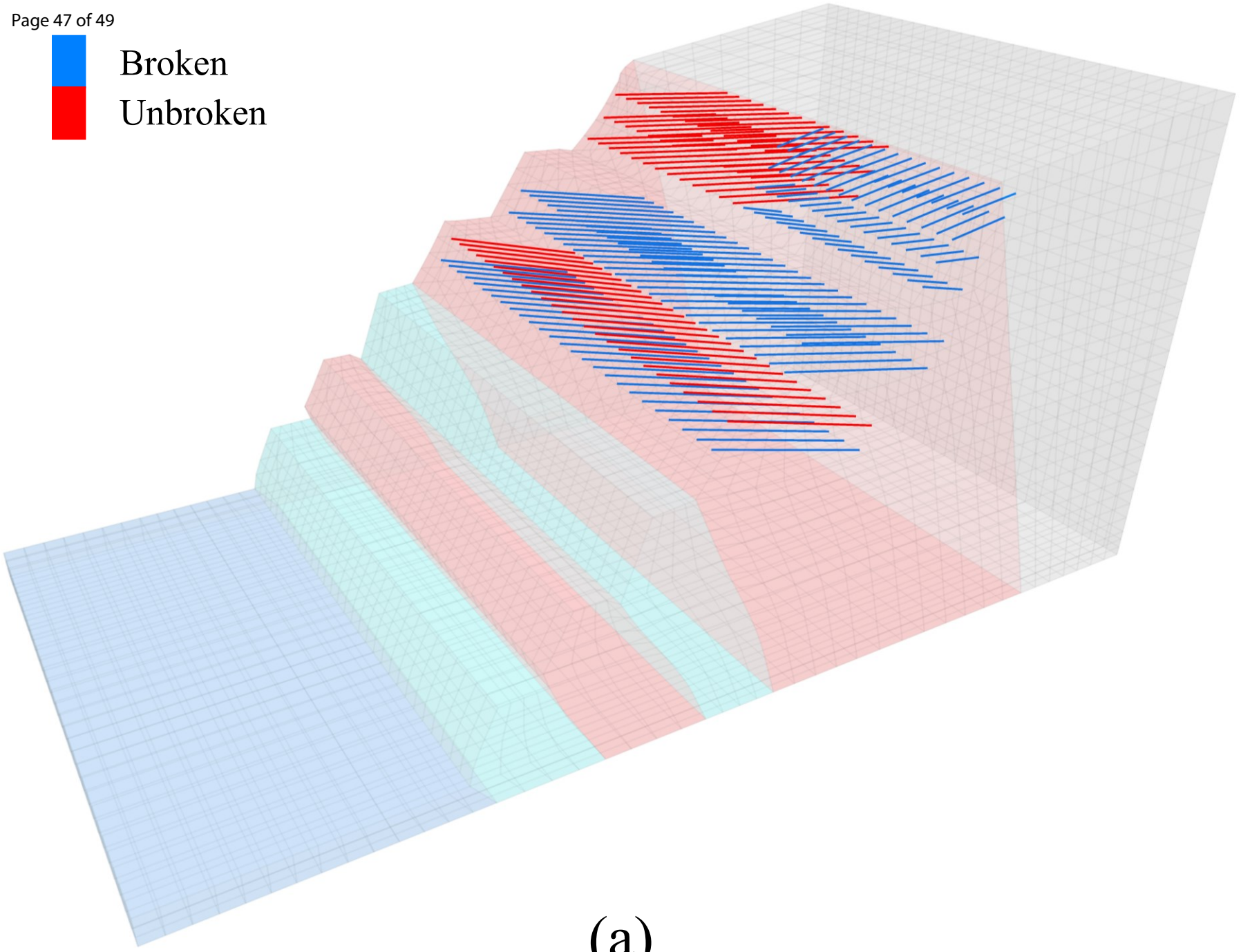

(a)

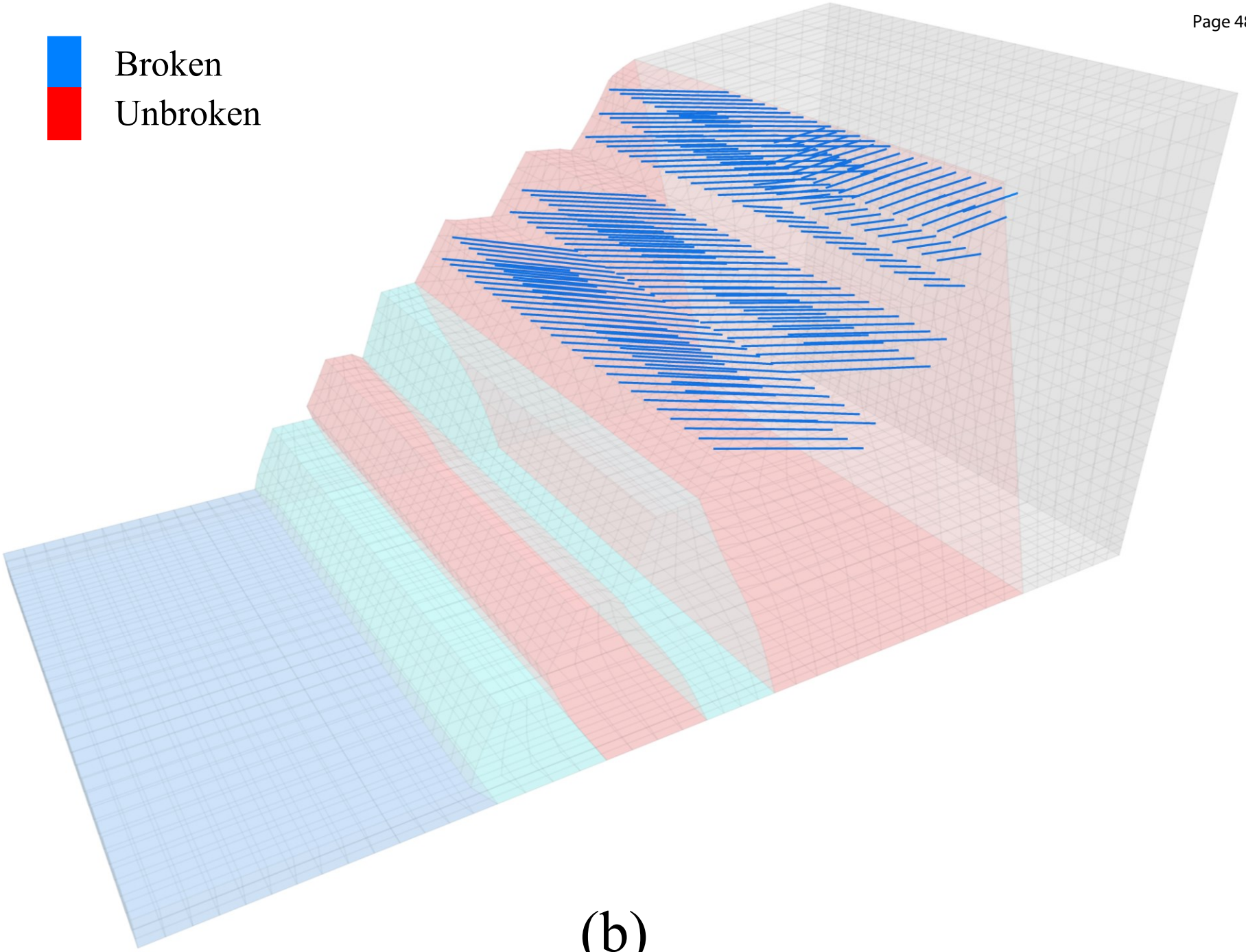

(b)

Appendix A1：

FISH code to calculate the global second-order work in FLAC3D software:

```
def global_D2W
global D2Wup = 0
global D2Wdown = 0
pnt = zone.head
loop while pnt # null
                D2Wup += zone.prop (pnt, 'd2w') * zone.vol (pnt)
                D2Wdown += zone.prop (pnt, 'norm_dsig') * zone.prop (pnt, 'norm_deps') * zone.vol (pnt)
pnt = zone.next (pnt)
end_loop
if D2Wdown <= 0.000000000000000001
                D2Wdown = 1
end_if
global global_D2W = D2Wup / D2Wdown
end
@global_D2W
```